Grantham Institute and Department of Earth Science and Engineering
Imperial College London

South Kensington Campus
London SW7 2AZ

Muhammad Hafeez Jeofry
PhD student

h.jeofry15@imperial.ac.uk

30 January 2018

Response to Reviewers' comments on manuscript #essd-2017-90

Dear Sir/Madam,

Many thanks for reviewing the above paper. The comments are positive, reasonable and helpful. We have revised and made some adjustments to the paper accordingly, and below we detail the changes that have been made.

We hope that the paper is now ready for publication in Earth System Science Data.

Sincerely,

Hafeez Jeofry (and on behalf of co-authors)

Referee #1

Line 24: "This has" or "These have"

Noted, however, the statement has been removed.

Lines 56-59: It's not clear what purpose this paragraph serves. Consider cutting.

Noted, the paragraph has been deleted.

Line 188: Your analysis, rather than RES, assumes this. RES can be done with other assumptions. Clarify.

Noted, the statement has been change to "*We assume Airborne RES propagates…*"

Line 343: Capitalize "Institute Ice Stream"

Noted, change has been made.

Referee #2

Line 187: An instrument cannot make assumptions, only its operators and those who interpret its data can. Further, the velocity used is an uncertainty of the order of 1%, because it depends on the well constrained but imperfectly known real part of the relative permittivity of pure ice and spatially variable densification. The mention of this velocity raises two important questions: 1. How is its (unstated) uncertainty incorporated into the error budget for the new bed topography? 2. Was this velocity used to correct the travel times between the surface and bed reflections for all datasets in this study? That's never explicitly stated. It certainly should be, and if different studies used different velocity values, then it's up to the present authors to make that important and necessary correction.

Noted, the statement has been change to "*We assume Airborne RES propagates…*"

All of the CReSIS, BAS GRADES/IMAGE and IMAFI surveys used a constant radio-wave speed of 0.168 m/ns. CReSIS OIB used 3.15 as the ice dielectric permittivity without considering the effect of firn on the top, so the radio wave speed in ice is c/sqrt (3.15), where c is the light speed in air. The thickness error using a constant ice dielectric permittivity is usually within ± 10 m at deep depth. Discussion about the thickness error for CReSIS OIB radar is discussed in "Coherent radar ice thickness measurements over the Greenland ice sheet (Gogineni et al.)". As for the BAS surveys, a nominal value of 10 m is used to correct for the firn layer during the processing of ice thickness and this introduces an error of the order of ±3 m.

In summary, we have made this issue clear in the text.

Line 210: I am a long-time MATLAB user and I do not know what is meant by MATLAB "standard format".

Noted, we have change the "standard format" to "data binary files".

Line 218: Again, what is the origin of this estimate? Further, an error map ought to be generated and shown for the bed topography.

The error was derived from the crossover analysis which showed that the RMS differences is 18.29 m ice thickness. The quoted RMS error should roughly approximate ±1% of total ice thickness. The purpose for the estimate is simply to acknowledge the error due to the firn layer and, so, we do not feel an error map needs to be generated.

Line 243-4: Explicitly state here that this is the same algorithm employed by Bedmap2, because it is somewhat primitive compared to that typically employed in the slow-moving sectors of Greenland, i.e., ordinary kriging.

Noted, changes have been made.

Line 252-3: Please reconsider significant figures here.

Noted, changes have been made.

Line 277: Where is the Pagano Shear Zone? It's not identified in Figure 1c.

Noted, we have removed "Pagano Shear Zone" from the text.

Line 292: The significance of a change in linear correlation coefficient can be easily calculated, and it ought to be done so if the term "significantly reduced" is to be used.

Noted, we have calculated the relative errors between the correlation coefficients of our new DEM and Bedmap2 product for each Profile. The relative errors are 2%, 1%, 12% and 13% for Profile A, B, C and D, respectively. The changes have been added to the text as well which is as follow:

"These value contrast with correlation coefficients from Bedmap2 of 0.87 for Profile C and 0.83 for Profile D, with relative errors of 12 and 13%, respectively."

Line 297-8: This statement contradicts the use of an outdated subaerial ice-surface DEM, i.e., the same as that of the Bedmap2. However, given the figures presented, the time to accomplish this task should not be significant. A newer Cryosat-2 DEM from Helm et al. (2014, The Cryosphere) ought to be employed, as it clearly demonstrates greater fidelity to high-resolution airborne altimetry than the ICESat/ERS-1/2 DEM that Bedmap2 employed (Table 2 of that study).

Point well made, however, no change has been made. There are two reasons why we did not consider the newer ice-surface Cryosat-2 DEM to compute the subglacial water pathway:

1. It is true that hydrology pathway is highly sensitive to ice-surface elevation relative to bed topography. However, by using the same ice-surface DEM to generate our new bed DEM as the ice-surface DEM used in Bedmap2, we are able to compute hydrology pathways and observe how the water routing has changed as a consequence of the new bed measurements (rather than ice surface change). In doing to, we are able to pinpoint several local small-scale differences in the water pathways between the respective bed topographies, which highlights hydraulic sensitivity in the region.
2. While the main product of this paper is the 1-km bed elevation DEM of the Weddell Sea sector, we also include 1-km ice thickness DEM of the Weddell Sea sector into the data repository, which allows others to modify or improve the DEM as new ice surface information appears. The bed elevation derived using mass conservation and kriging, as shown in figure 3e, is an example of how we can further improve the DEM.

Line 315-322: The geographic coordinates of the lakes do not need to be mentioned, and if a graticule were added to Figure 1c they would become even more unnecessary. Further, this paragraph doesn't really add much information about the lakes that is not available from existing inventories. It simply enumerates them. Reconsider.

Noted, we have deleted the geographic coordinates and include the graticule to Figure 1c.

Line 332-333: This statement about Bungenstock Ice Rise being a good example of one is not very meaningful.

Noted, we have deleted the statement.

Line 336-337: This statement is wrong. There are very clear metrics for measuring surface roughness, independent of FFTs. Shepard et al. (2001, JGR) summarizes them very nicely, and they have been employed in several glaciological studies of ice-sheet beds (e.g., Young et al., 2011, Nature; MacGregor et al., 2013, JGlac).

Point well made, we have deleted "*Although there is no specific method or standardized unit to measure bed roughness,*".

Figures & Tables

All the figures in this study need significant improvements.
Figure 1. (a) Add a scale bar, the grounding line and a colour bar for the surface velocity. (b) Add a legend for all the different surveys. (c). This panel is quite hard to read. The black labels on a dark gray background do not work well. Brighten MOA and increase the contrast. It is mentioned in the text that different grounding lines exist, and all should be shown on this figure. Also, a distinct symbology should be used for different types of features (e.g., lakes vs. troughs, rather than using the same white dot for everything.

Figure 1a – We have added the scale bar, the MOA grounding line and the colour bar for the surface velocity.
Figure 1b – We have added the legend.
Figure 1c – We have added a white background to the labels, and we have added all four grounding lines. Note that we did not put legends of the different grounding lines due to limited space on the figure. However, we have explained and distinguished the different grounding lines based on its colour in the caption. Finally, we used a different symbology for lakes (white dot) and troughs (white asterisk). A graticule has also been added.

Figure 2. It is very difficult to make out much of anything on the lower radargram. Adjust its colour scale.

Noted, we have adjusted the colour scale of the lower radargram.

Figure 3. (a,b) I recommend using the USGS color scale for topography instead. Demcmap in MATLAB. The bizarre irregular intervals for the colour scale are unacceptable. Use simple, regular intervals, e.g., –2000:200:600 in MATLAB form. (c) Again, fix the weird irregular intervals. I'm not sure why the red/blue color scale with yellow was invented, but it should be replaced with one that has red/blue with white in the middle. Much more intuitive.

We have adjusted the interval for figure 3a and 3b using -2000:200:600 and for figure 3c using -350:50:350 intervals. However, no change has been made to the colour scale itself. We have tried the suggested colour scale, but it is not appealing to us and we have no problem with the current colour scale.

Figure 4. Add a legend. There's plenty of room for one. These figures aren't information-dense, so generate them closer together.

We have added the legends in each profile figure and have arranged them close together.

Grammar

Line 121: C-130R or LC-130?

Noted, it is LC-130, change has been made.

Line 143: I do not understand why "chirp" is capitalized here

Noted, change has been made.

Line 165: to be 7 cm

Noted, change has been made.

Line 200: radar shot number that is used

Noted, change has been made.

Line 210: MATLAB should be capitalized

Noted, change has been made.

Line 279: Here and throughout the manuscript, capitalize all proper noun geographic locations, e.g., Institute Ice Stream

Noted, change has been made.

Line 345: Passive voice: "It is considered. . ."

Noted, however, no change has been made.

#Further editing

Major Issues

1.

We have added a new method in section 4.4 "Inferring bed elevation using mass conservation (MC) and Kriging" and a new figure 3e which is the modified version of our new bed elevation DEM product using MC at the fast-flowing region of ice and Kriging at the slow-moving ice:

"Relying on the conservation of mass (MC) to infer the bed between flight lines (Morlighem et al., 2011), we were able to investigate how the bed can be developed further in fast-flowing regions, using a new interpolation technique. To perform the MC procedure, we used InSAR-derived surface velocities from Rignot et al. (2011b), surface mass balance from RACMO 2.3 (Van Wessem et al., 2014), and assumed that the ice thinning/thickening rate and basal melt are negligible. We constrained the optimization with ground penetrating radar from CReSIS, GRADES, IMAFI and SPRI, described above, and used a mesh horizontal resolution of 500 m."

The purpose of this added product is to demonstrate that there are many ways that our new DEM can be used and modified according to their interpretations of the ice-sheet dynamic in the WS sector region. We have added a new paragraph explaining the details of the new product in section 5.1:

"The new DEM can be refined further to deal with bumps and irregularities associated with interpolation effects from along-track data in otherwise data sparse regions. We used mass conservation (MC) and kriging to infer the bed elevation (Fig. 3e) beneath the fast and slow-moving ice, respectively, similar to that successfully employed in Greenland (Morlighem et al., 2017). In general, the bed elevation derived from MC and kriging is consistent with our new DEM. However, there are significant changes in the bed morphology beneath fast flowing ice. For example, the tributary of the Foundation Ice Stream has been extended for ~100 km further inland relative to our new DEM."

2.

We have made corrections to account for the way Bedmap2 is projected using the gl04c geoid. (Bedmap2 was produced relative to the gl04c geoid to allow realistic numerical modelling by incorporating the role of relative sea level / glacial isostatic adjustment.) In a previous figure, we did not correct the datum and, so, it was not strictly comparable with our new DEM, because this is produced relative to the WGS 1984 Antarctic Polar Stereographic projection. We have made the necessary corrections by transforming Bedmap2 onto the WGS 1984 Antarctic Polar Stereographic. Consequently, we have reproduced the figure 3c "Difference map" and figure 4. The re-analysis does not have a major difference relative to the previous figures, however. Finally, we have made the necessary adjustments to the figures, and have added text into the methodology section 4.3 as follows:

"The Bedmap2 bed elevation product (Fretwell et al., 2013) was transformed from the gl04c geoid projection to the WGS 1984 Antarctic Polar Stereographic projection."

Minor Issues

Line 21: "update" to "improve"

Line 23-24: "as BEDMAP2 included only relatively crude ice thickness measurements determined in the field for quality control" to "from the relatively crude measurements determined in the field for quality control purposes used in Bedmap2".

Line 24-25: "This have resulted in the deep parts of the topography not being visible in the fieldwork non-SAR processed radargrams" deleted.

Line 26: "deep trough" to "deep subglacial trough".

Line 28: “at the ice-bed interface” deleted.

Line 29: “sensitivity” to “potential vulnerability”.

Line 29: “of the ice sheet” deleted.

Line 32: “in the” to “at”.

Line 37: “projected” to “concluded”.

Line 41: “in places more than” added.

Line 43: “future” deleted.

Line 44: “project” to “show”.

Line 46: “similar manner” to “manner similar”.

Line 48-49: “from the parent ice mass” deleted.

Line 49: “together” deleted.

Line 62: “entire” deleted.

Line 64: “late 1960s and..” added.

Line 66: “and” deleted.

Line 66: “thickness” to “ice thickness”

Line 68: “highly” deleted.

Line 74: “line representation” to “lines compared”.

Line 74: “observations” to “satellite-derived observations”.

Line 75: “limited” to “restricted”.

Line 75: “to the community” deleted.

Line 77: “project” to “compilation”.

Line 79: “where only 34% of cells have data and 80% have data within the range of 20 km” deleted.

Line 85: “improving knowledge of the land surface beneath the ice sheet. This…” to “…,which…”

Line 87: “the” deleted.

Line 87: “of” to “associated with”.

Line 88: “in glaciology” added.

Line 90: “a revised” to “an improved”.

Line 96: “The study area is located in” deleted.

Line 96: “covering” to “covers”.

Line 97: “The DEM” to “The region covered by the DEM”.

Line 98: “with the” to “with”.

Line 102: “We used the Differential Interferometry Synthetic Aperture Radar (DInSAR) grounding line (Rignot et al., 2011b) to delimit the ice shelf-facing margin of our grid” added.

Line 102-107: “The data and methods used in this study are mostly similar to Jeofry et al. (2017), however, we have expanded the boundaries of our new bed elevation DEM by focussing across the Weddell Sea sector relative to the Institute ice stream as the main focus in Jeofry et al. (2017). In addition, this paper focuses on discussing the geomorphology and improvement that have been made between our new bed elevation DEM and Bedmap2 product whereas Jeofry et al. (2017) discuss on the hitherto unknown subglacial embayment and its effect to the ice sheet dynamics” deleted.

Line 120: “of the 1970s” deleted.

Line 132: “was” to “were”.

Line 133: “was” to “were”.

Line 134: “records were” to “record was”.

Line 144: “is” to “are”.

Line 157: the coordinate for C110 “-82º 37’ 30’’ N, 280º 59’ 13.2’’E” has been removed. It has been replaced with “*17 flights were flown from C110, which is located above Institute E2 subglacial lake,…*”.

Line 158: the coordinate for Patriot Hills “-80º 19’ 60’’ N, 278º 34’ 60’’E” has been removed.

Line 199: “200m” to “200 m”.

Line 247-249: “The ice thickness DEM was then subtracted from the ice-sheet surface elevation derived from the combined European Remote Sensing Satellite-1 (ERS-1) radar and Ice, Cloud and land Elevation Satellite (ICESat) laser satellite altimetry DEM (Bamber et al., 2009a), to derive the bed topography” to “The ice thickness DEM was then subtracted from the ice-sheet surface elevation DEM (from European Remote Sensing Satellite-1 (ERS-1) radar and Ice, Cloud and land Elevation Satellite (ICESat) laser satellite altimetry datasets (Bamber et al., 2009a)), to derive the bed topography”.

Line 289: “the” deleted.

Line 291: “the” deleted.

Line 298: “It is noted that” deleted.

Line 304: “this is” deleted.

Line 310: “almost” deleted.

Line 312: “a vital constituent” to “an obvious component”.

Line 313: “melts” to “allows”

Line 314: “to melt if it is >~2km” added.

Line 314: “on the bed” added.

Line 314: “of the ice” deleted.

Line 315: “At the western margin of the Ellsworth Mountain” to “West of the Ellsworth Mountain”.

Line 315: “large” deleted.

Line 317: “In some cases, ice-surface elevation changes have been linked with subglacial lake hydrological change (Siegert et al., 2016a) – the so called ‘active’ subglacial lakes.” Added.

Line 317: “active” added.

Line 318: “The” deleted

Line 319: “The” deleted.

Line 321: “active” added.

Line 323: “East of the Foundation Ice Stream, there are 16 active subglacial lakes distributed along the main trunk of Academy Ice Stream (Wright and Siegert, 2012)” added.

Line 340: “of the” deleted.

Line 343: “and its connection” to “and connects”.

Line 350: “It is worth noting that the lake is outside the grid of our new DEM” added.

Line 385: “in the” to “at”.

Line 416: “the Institute ice stream, Bungenstock ice rise, Möller and Foundation ice streams” to “the Institute, Möller and Foundation ice streams, and the Bungenstock ice rise”.

Line 417: “between the new DEM and that of the previous DEM of the region (Bedmap2)” to “between the new and previous DEMs (i.e., Bedmap2)”

Line 419-421: “the bed elevation of our DEM appears to be slightly lower relative to the bed elevation of Bedmap2 DEM, which is likely the results of the deep sections of the topography not being visible in the fieldwork non-SAR processed radargrams” to “improved processing of existing data has led to some particularly deep regions of bed to be better resolved than in Bedmap2”

Line 422: “that derived from” deleted.

A new bed elevation model for the Weddell Sea sector of the West Antarctic Ice Sheet

Hafeez Jeofry[1,2], Neil Ross[3], Hugh F.J. Corr[4], Jilu Li[5], Mathieu Morlighem[6], Prasad Gogineni[7] and Martin J. Siegert[1]

[1] Grantham Institute and Department of Earth Science and Engineering, Imperial College London, South Kensington, London, UK
[2] School of Marine Science and Environment, Universiti Malaysia Terengganu, Kuala Terengganu, Terengganu, Malaysia
[3] School of Geography, Politics and Sociology, Newcastle University, Claremont Road, Newcastle Upon Tyne, UK
[4] British Antarctic Survey, Natural Environment Research Council, Cambridge, UK
[5] Center for the Remote Sensing of Ice Sheets, University of Kansas, Lawrence, Kansas, USA
[6] Department of Earth System Science, University of California, Irvine, California, USA
[7] ECE Department, The University of Alabama, Tuscaloosa, AL 35487, USA

Correspondence to: Hafeez Jeofry (h.jeofry15@imperial.ac.uk) and Martin Siegert (m.siegert@imperial.ac.uk)

Abstract. We present a new bed elevation digital elevation model (DEM), with a 1 km spatial resolution, for the Weddell Sea sector of the West Antarctic Ice Sheet. The DEM has a total area of ~125,000 km^2 covering the Institute, Möller and Foundation Ice Streams and the Bungenstock ice rise. In comparison with the Bedmap2 product, our DEM includes new aerogeophysical datasets acquired by the Center for Remote Sensing of Ice Sheets (CReSIS) through the NASA Operation IceBridge (OIB) program in 2012, 2014 and 2016. We also improve bed elevation information from the single largest existing dataset in the region, collected by the British Antarctic Survey (BAS) Polarimetric Airborne Survey Instrument (PASIN) in 2010-11, from the relatively crude measurements determined in the field for quality control purposes used in Bedmap2. While the gross form of the new DEM is similar to Bedmap2, there are some notable differences. For example, the position and size of a deep subglacial trough (~2 km below sea level) between the ice sheet interior and the grounding line of Foundation Ice Stream has been redefined. From the revised DEM, we are able to better derive the expected routing of basal water and, by comparison with that calculated using Bedmap2, we are able to assess regions where hydraulic flow is sensitive to change. Given the potential vulnerability of this sector to ocean-induced melting at the grounding line, especially in light of improved definition of the Foundation Ice Stream trough, our revised DEM will be of value to ice-sheet modelling in efforts to quantify future glaciological changes in the region and, from this, the potential impact on global sea level. The new 1 km bed elevation product of the Weddell Sea sector, West Antarctica can be found at http://doi.org/10.5281/zenodo.1035488.

1. Introduction

The Intergovernmental Panel on Climate Change (IPCC) concluded that global sea level could increase by between 0.26 and 0.82 m by the end of the 21st century (Stocker, 2014). The rising oceans pose a threat to the socio-economic activities of hundreds of millions of people, mostly in Asia, living at and close to the coastal environment. Several processes drive sea level rise (e.g. thermal expansion of the oceans), but the largest potential factor comes from the ice sheets in Antarctica. The West Antarctic Ice Sheet (WAIS), which if melted would raise sea-level by around 3.5 m, is grounded on a bed which is in places more than 2 km below sea level (Bamber et al., 2009b; Ross et al., 2012; Fretwell et al., 2013), allowing the ice margin to have direct contact with ocean water. One of the most sensitive regions of the WAIS to potential ocean warming is the Weddell Sea (WS) sector (Ross et al., 2012; Wright et al., 2014). Ocean modelling studies show that changes in present ocean circulation could bring warm ocean water into direct contact with the grounding lines at the base of the Filchner Ronne Ice Shelf (FRIS) (Hellmer et al., 2012; Wright et al., 2014; Martin et al., 2015; Ritz et al., 2015; Thoma et al., 2015), which would act in a manner similar to the ocean-induced basal melting under the Pine Island Glacier ice shelf (Jacobs et al., 2011). Enhanced melting of the FRIS could lead to a decrease in the buttressing support to the upstream grounded ice, encouraging enhanced flow to the ocean (Jacobs et al., 2011). A recent modelling study, using a general ocean circulation model coupled with a 3D thermodynamic ice sheet model, simulated the inflow of warm ocean water into the Ronne-Filchner ice shelf cavity on a 1000 year timescale (Thoma et al., 2015). A second modelling study, this time using an ice sheet model, indicated that the Institute and Möller Ice Streams are highly sensitive to melting at the grounding lines; with grounding line retreat up to 180 km possible

across the Institute and Möller Ice Streams (Wright et al., 2014). While the Foundation Ice Stream was shown to be relatively resistant to ocean-induced change (Wright et al., 2014), a dearth of geophysical measurements of ice thickness across the ice stream at the time means the result may be inaccurate.

The primary tool for measurements of subglacial topography and basal ice-sheet conditions is radio-echo sounding (RES) (Dowdeswell and Evans, 2004; Bingham and Siegert, 2007).The first topographic representation of the land surface beneath the Antarctic ice sheet (Drewry, 1983) was published by the Scott Polar Research Institute, University of Cambridge, (SPRI) in collaboration with the US National Science Foundation Division of Polar Programmes (NSF-DPP) and the Technical University of Denmark (TUD), following multiple field seasons of RES surveying in the late 1960s and 1970s (Drewry and Meldrum, 1978; Drewry et al., 1980; Jankowski and Drewry, 1981; Drewry, 1983). The compilation included folio maps of bed topography, ice-sheet surface elevation and ice thickness. The bed was digitized on a 20 km grid for use in ice-sheet modelling (Budd et al., 1984). However, only around one third of the continent was measured at a line spacing of less than ~100 km (Lythe and Vaughan, 2001), making the elevation product erroneous in many places, with obvious knock-on consequences for modelling. Several RES campaigns were thenceforth conducted, and data from them were compiled into a single new Antarctic bed elevation product, named Bedmap (Lythe and Vaughan, 2001). The Bedmap DEM had a cell resolution of 5 km, and included over 1.4 million km and 250,000 km line track of airborne and ground-based radio-echo sounding data, respectively. Subglacial topography was extended north to 60^0S, for purposes of ice sheet modelling, and determination of ice-ocean interactions. Since its release, Bedmap has proved to be highly useful for a wide range of research, yet inherent errors within it (e.g. inaccuracies in the DEM and conflicting grounding lines compared with satellite-derived observations) restricted its effectiveness (Le Brocq et al., 2010; Fretwell et al., 2013). After 2001, several new RES surveys were conducted to fill data gaps revealed by Bedmap, especially during and after the 4th International Polar Year (2007-9). These new data led to the most recent Antarctic bed compilation, named Bedmap2 (Fretwell et al., 2013). Despite significant improvements in the resolution and accuracy of Bedmap2 compared with Bedmap, a number of inaccuracies and poorly sampled areas persist (Fretwell et al., 2013; Pritchard, 2014), preventing a comprehensive appreciation of the complex relation between the topography and internal ice-sheet processes, and indeed a full appreciation of the sensitivity of the Antarctic ice sheet to ocean and atmospheric warming.

The Weddell Sea sector of the WAIS was the subject of a major aerogeophysical survey in 2010-11 (Ross et al., 2012), revealing the ~2 km deep Robin Subglacial Basin immediately upstream of present-day grounding lines, from which confirmation of the ice-sheet sensitivity from ice-sheet modelling was determined (Wright et al., 2014). Further geophysical surveying of the region has been undertaken since Bedmap2 (Ross et al., 2012), which has provided an enhanced appreciation of the importance of basal hydrology to ice flow (Siegert et al., 2016b) and complexities associated with the interaction of basal water flow, bed topography and ice-surface elevation (Lindbäck et al., 2014; Siegert et al., 2014; Graham et al., 2016), emphasising the importance of developing accurate and high resolution DEMs in glaciology.

In this paper, we present an improved bed DEM for the Weddell Sea sector, based on a compilation of new airborne radar surveys. The DEM has a total area of ~125,000 km^2 and a grid cell resolution of 1 km. From this dataset, we reveal the expected pathways of subglacial water, and discuss the differences between the new DEM and Bedmap2.

2. Study area

The Weddell Sea sector of WAIS covers the Institute, Möller and Foundation Ice Streams, and the Bungenstock ice rise (Fig. 1). The region covered by the DEM extends 135 km grid south of the Bungenstock ice rise, 195 km grid east of the Foundation Ice Stream, over the Pensacola Mountain and 185 km grid west of the Institute Ice Stream. In comparison with Bedmap2, our new DEM benefits from several new airborne geophysical datasets (e.g. NASA OIB 2012, 2014 and 2016). In addition, the new DEM is improved by the inclusion of ice thickness picks derived from SAR-processed RES data from the BAS aerogeophysical survey of the Institute and Möller Ice Streams conducted in 2010/2011. This has improved the accuracy of the determination of the ice bed interface in comparison to Bedmap2. We used the Differential Interferometry Synthetic Aperture Radar (DInSAR) grounding line (Rignot et al., 2011c) to delimit the ice shelf-facing margin of our grid.

3. Data and methods

The RES data used in this study were compiled from four main sources (Fig. 1a). First, SPRI data collected during six survey campaigns between 1969 and 1979 (Drewry, 1983). Second, the BAS airborne radar survey accomplished during the austral summer 2006/07 (GRADES/IMAGE) (Ashmore et al., 2014). Third, the BAS survey of the Institute and Möller Ice Streams, undertaken in 2010/2011 (IMAFI) (Ross et al., 2012). Fourth, flights conducted by the Center for the Remote Sensing of Ice Sheet (CReSIS) during the NASA OIB programme in 2012, 2014 and 2016 (Gogineni, 2012) supplement the data previously used in the Bedmap2 bed elevation product to accurately characterize the subglacial topography of this part of the Weddell Sea sector.

3.1 Scott Polar Research Institute survey

The SPRI surveys covered a total area of 6.96 million km^2 (~40% of continental area) across West and East Antarctica (Drewry et al., 1980). The data were collected using a pulsed radar system operating at centre frequencies of 60 and 300 MHz (Christensen, 1970; Skou and Søndergaard, 1976) equipped on NSF LC-130 Hercules aircraft (Drewry and Meldrum, 1978; Drewry et al., 1980; Jankowski and Drewry, 1981; Drewry, 1983). The 60 MHz antennas, built by the Technical University of Denmark, comprised an array of four half wave dipoles, which were mounted in neutral aerofoil architecture of insulating components beneath the starboard wing. The 300 MHz antennas were composed of four dipoles attached underneath a reflector panel below the port wing. The purpose of this unique design was to improve the backscatter acquisition and directivity. The returned signals were archived on 35 mm film and dry-silver paper by a fibre optic oscillograph. Aircraft navigation was assisted using an LTN-51 inertial navigation system giving a positional error of around 3 km. Navigation and other flight data were stored on magnetic and analogue tape by an Airborne Research Data System (ARDS) constructed by US Naval Weapons Center. The system recorded up to 100 channels of six-digit data with a sampling rate of 303 Hz per channel. Navigation, ice thickness and ice surface elevation records were recorded every 20 seconds, corresponding to around 1.6 km between each data point included on the Bedmap2 product. The data were initially recorded on a 35-mm photographic film (i.e. Z-scope radargrams) and were later scanned and digitized, as part of a NERC Centre for Polar Observation and Modelling (CPOM), in 2004. Each film record was scanned separately and reformatted to form a single electronic image of a RES transect. The scanned image was loaded into an image analysis package (i.e. ERDAS Imagine) to trace the internal layers which were then digitized. The dataset was later standardized with respect to the ice surface.

3.2 BAS GRADES/IMAGE surveys

The GRADES/IMAGE project was conducted during the austral summer of 2006/2007 and consisted of ~27,550 km of RES data flown across the Antarctic Peninsula, Ellsworth Mountain and Filchner-Ronne ice shelf. The BAS Polarimetric radar Airborne Science Instrument (PASIN) radar operates at a centre frequency of 150 MHz, has a 10 MHz bandwidth and a pulse-coded waveform acquisition rate of 312.5 Hz (Corr et al., 2007; Ashmore et al., 2014). The PASIN system interleaves a pulse and chirp signal to acquire two datasets simultaneously. Pulse data are used for imaging layering in the upper half of the ice column, whilst the more powerful chirp is used for imaging the deep-ice and sounding the ice sheet bed. The peak transmitted power of the system is 4 kW. The spatial sampling interval of ~20 m resulted in ~50,000 traces of data for a typical 4.5-hour flight. The radar system consisted of 8 folded dipole elements; 4 transmitters on the port side and 4 receivers on the starboard side. The receiving "backscatter" signal was digitized and sampled using a sub-Nyquist sampling technique and are then recorded on magnetic tape drives. The pulses are compressed using a matched filter, and sidelobes are minimized using a Blackman window. Aircraft position was recorded by an onboard carrier wave global positioning system (GPS). The absolute positional accuracy for GRADES/IMAGE was 0.1 m (Corr et al., 2007). Synthetic Aperture Radar (SAR) processing was not applied to the GRADES/IMAGE data.

3.3 BAS Institute-Möller Antarctic Funding Initiative surveys

The BAS data acquired during the IMAFI project consist of ~25,000 km of aerogeophysical data collected during 27 flights from two field camps. 17 flights were flown from C110, which is located above Institute E2 subglacial lake, and the remaining 10 flights were flown from Patriot Hills (Fig. 1b). Data were acquired with the same PASIN radar used for the GRADES/IMAGE survey. The data rate of 13 Hz gave a spatial sampling interval of ~10 m for IMAFI. The system was installed on the BAS de Havilland Twin Otter aircraft with a four-element folded dipole array mounted below the starboard wing used for reception and the identical array attached below the port wing for transmission. The flights were flown in a stepped pattern during the IMAFI survey to optimise potential field data (gravity and magnetics) acquisition (Fig. 1a). Leica 500 and Novatel DL-V3 GPS receivers were installed in the aircraft, corrected with two Leica 500 GPS base stations which were operated throughout the survey to calculate the position of the aircraft (Jordan et al., 2013). The positional data were referenced to the WGS 84 ellipsoid. The absolute positional accuracy for IMAFI (the standard deviation for the GPS positional error) was calculated to be 7 cm and 20 cm in the horizontal and vertical dimensions (Jordan et al., 2013). 2-D focused SAR processing (Hélière et al., 2007) (see section 4.1) was applied to the IMAFI data.

3.4 NASA OIB / CReSIS surveys

The OIB project surveyed a total distance of ~32,693 km, ~52460 km and ~53672 km in Antarctica in 2012, 2014 and 2016, respectively, using the Multichannel Coherent Radar Depth Sounder (MCoRDS) system developed at the University of Kansas (Gogineni, 2012). The system was operated with a carrier frequency of 195 MHz, a bandwidth of 10 MHz and 50 MHz in

2012 (Rodriguez-Morales et al., 2014) and 2014 onwards (Siegert et al., 2016b). The radar consisted of a five – element antenna array housed in a customized antenna fairing which is attached beneath the NASA DC – 8 aircraft fuselage (Rodriguez-Morales et al., 2014). The five antennas were operated from a multichannel digital direct synthesis (DDS) controlled waveform generator enabling the user to adjust the frequency, timing, amplitude and phase of each transmitted waveform (Shi et al., 2010). The radar employs an eight-channel waveform generator to emit eight independent transmit chirp pulses. The system is capable of supporting 5 receiver channels with Analog Devices AD9640 14 bit analog-to-digital converter (ADC) acquiring the waveform at a rate of 111 MHz in 2012 (Gogineni, 2012). The system was upgraded in 2014 and 2016 utilizing six channel chirp generation and supports six receiver channels with a waveform acquisition rate at 150 MHz. Multiple receivers allow array processing to suppress surface clutter in the cross track direction which could potentially conceal weak echoes from the ice – bed interface (Rodriguez-Morales et al., 2014). The radar data are synchronized with the GPS and inertial navigation system (INS) using the GPS time stamp to determine the location of data acquisition.

4. Data processing

We assume airborne RES propagates through ice at a constant wave speed of 0.168 m ns^{-1}, since glacial ice is assumed to be homogenous (Lythe and Vaughan, 2001; Plewes and Hubbard, 2001; Dowdeswell and Evans, 2004). The radar pulse travels through a medium until it meets a boundary of differing dielectric constant, which causes some of the radio wave to be reflected and subsequently captured by the receiver antenna. There are three factors causing dielectric contrast in ice sheets; density variations in the upper 700 m, acidic layers caused by the aerosol from volcanic activity, and ice permittivity variations from crystal fabrics (Siegert, 1999; Corr et al., 2007). The time travelled by the radar pulse between the upper and lower reflecting surface is measured and converted to ice thickness with reference to WGS 84 (Fig. 2). The digitized SPRI-NSF-TUD bed picks data are available through the BAS webpage (https://data.bas.ac.uk/metadata.php?id=GB/NERC/BAS/AEDC/00326). The two-dimensional SAR-processed radargrams in SEG-Y format for the IMAFI survey are provided at doi.org/10.5285/8a975b9e-f18c-4c51-9bdb-b00b82da52b8, whereas the ice thickness datasets in Comma Separated Value (CSV) format for both GRADES/IMAGE and IMAFI are available via the BAS aerogeophysical processing portal (https://secure.antarctica.ac.uk/data/aerogeo/). The ice thickness data for IMAFI are provided in two folders; (1) the region of thinner ice (<200 m) picked from the pulse dataset and (2) the overall ice thickness data, derived from picking of SAR-processed chirp radargrams. The data are arranged according to the latitude, longitude, ice thickness values and the pulse repetition interval (PRI) radar shot number that is used to index the raw data. The OIB SAR images (Level 1B) in MAT (binary MATLAB) format and the radar depth sounder Level 2 (L2) data in CSV format are available via the CReSIS website (https://data.cresis.ku.edu/). The L2 data include measurements for GPS time during data collection, latitude, longitude, elevation, surface, bottom and thickness. For more information on these data, the reader should refer to the appropriate CReSIS data information and guidance notes for each field season (i.e. https://data.cresis.ku.edu/data/rds/rds_readme.pdf).

4.1 GRADES/IMAGE and Institute-Möller Antarctic Funding Initiative data processing

The waveform was retrieved and sequenced according to its respective transmit pulse type. The modified data were then collated using MATLAB data binary files. Doppler filtering (Hélière et al., 2007) was used to remove the backscattering hyperbola in the along-track direction (Corr et al., 2007; Ross et al., 2012). Chirp compression was then applied to the along-track data. Unfocused synthetic aperture (SAR) processing was used for the GRADES/IMAGE survey by applying a moving average of 33 data points (Corr et al., 2007) whereas 2D-SAR (i.e. focused) processing based on Omega-K algorithm was used to process the IMAFI data (Hélière et al., 2007; Winter et al., 2015) to enhance both along-track resolution and echo signal noise. The bed echo was depicted in a semi-automatic manner using PROMAX seismic processing software. All picking for IMAFI was undertaken by a single operator (Neil Ross). A nominal value of 10 m is used to correct for the firn layer during the processing of ice thickness, which introduces an error of the order of $\pm$ 3 m across the survey field (Ross et al., 2012). This is small relative to the total error budget of the order of $\pm$ 1%. Finally, the GPS and RES data were combined to determine the ice thickness, ice-surface and bed elevation datasets. Elevations are measured with reference to WGS84. The ice surface elevation was calculated by subtracting terrain clearance from the height of the aircraft, whereas the bed elevation was computed by subtracting the ice thickness from the ice surface elevation.

4.2 OIB data processing

The OIB radar adopts SAR processing in the along-track direction to provide higher resolution images of the subglacial profile. The data were processed in three steps to improve the signal-to-noise ratio and increase the along-track resolution (Gogineni et al., 2014). The raw data were first converted from a digital quantization level to a receiver voltage level. The surface was captured using the low-gain data, microwave radar or laser altimeter. A normalized matched filter with frequency-domain

windowing was then used for pulse compression. 2D-SAR processing was used after conditioning the data, which is based on the frequency-wavenumber (F-K) algorithm. The F-K SAR processing, however, requires a straight and uniformly sampled data which are usually not met in the raw data since the aircraft's speed is not consistent and the trajectory is not straight. The raw data were thus spatially resampled along-track using a sinc kernel to approximate a uniformly sampled dataset. The vertical deviation in aircraft trajectory from the horizontal flight path was compensated in the frequency domain with a time-delay phase shift. The phase shift was later removed for array processing as it is able to account for the non-uniform sampling; the purpose is to maintain the original geometry for the array processing. Array processing was performed in the cross-track flightpath to reduce surface clutter as well as improving the signal-to-noise ratio. Both the delay-and-sum and Minimum Variance Distortionless Response (MVDR) beamformer were used to combine the multichannel data, and for regions with significant surface clutter the MVDR beamformer could effectively minimize the clutter power and pass the desired signal with optimum weights (Harry and Trees, 2002).

4.3 Quantifying ice thickness, bed topography and subglacial water flow

The new ice thickness DEM was formed from all the available RES data using the 'Topo to Raster' function in ArcGIS, based on the Australian National University Digital Elevation Model (ANUDEM) elevation gridding algorithm (Hutchinson, 1988). This is the same algorithm employed by Bedmap2. The ice thickness picks from the geophysical data were gridded using the Nearest Neighbour interpolation within Topo to Raster. The ice thickness DEM was then subtracted from the ice-sheet surface elevation DEM (from European Remote Sensing Satellite-1 (ERS-1) radar and Ice, Cloud and land Elevation Satellite (ICESat) laser satellite altimetry datasets (Bamber et al., 2009a)), to derive the bed topography. The ice thickness, ice-sheet surface and bed elevations were then gridded at a uniform 1 km spacing, and referenced to the Polar Stereographic projection (Snyder, 1987) to form the new DEMs. The Bedmap2 bed elevation product (Fretwell et al., 2013) was transformed from the gl04c geoid projection to the WGS 1984 Antarctic Polar Stereographic projection. The difference map between the new DEM and the Bedmap2 product was computed by subtracting the Bedmap2 bed elevation DEM from the new bed elevation DEM. Crossover analysis for the 2006/7 data onwards (including data acquired on flightlines beyond the extent of our DEM) shows the RMS errors of 9.1 m (GRADES/IMAGE), 15.8 m (IMAFI), 45.9 m (CRESIS 2012), 23.7 m (CRESIS 2014) and 20.3 m (CRESIS 2016).

Subglacial water flowpaths were calculated based on the hydraulic potentiometric surface principle, in which basal water pressure is balanced by the ice overburden pressure as follows:

$$\varphi = (\rho_w \times g \times y) + (\rho_i \times g \times h) \quad (1)$$

where φ is the theoretical hydropotential surface, y is the bed elevation, h is the ice thickness, ρ_w and ρ_i are the density of water (1000 kg m^{-3}) and ice (920 kg m^{-3}), assuming ice to be homogenous, respectively, and g is the gravitational constant (9.81 ms^{-2}) (Shreve, 1972). Sinks in the hydrostatic pressure field raster were filled to produce realistic hydrologic flowpaths. The 'flow direction' of the raster was then defined by assigning each cell a direction to the steepest downslope neighbouring cell. Sub-basins less than 200 km^2 were removed due to the coarse input of bed topography and ice thickness DEMs.

4.4 Inferring bed elevation using mass conservation (MC) and Kriging

Relying on the conservation of mass (MC) to infer the bed between flight lines (Morlighem et al., 2011), we were able to investigate how the bed can be developed further in fast-flowing regions, using a new interpolation technique. To perform the MC procedure, we used InSAR-derived surface velocities from Rignot et al. (2011b), surface mass balance from RACMO 2.3 (Van Wessem et al., 2014), and assumed that the ice thinning/thickening rate and basal melt are negligible. We constrained the optimization with ground penetrating radar from CReSIS, GRADES, IMAFI and SPRI, described above, and used a mesh horizontal resolution of 500 m.

5. Results

5.1 A new 1-km digital elevation model of the Weddell Sea sector

We present a new DEM of the WS sector of West Antarctica, compiled from several airborne geophysical radar surveys (Fig. 3a). The Bedmap2 bed elevation and the difference map are shown in Fig. 3b and 3c respectively. The new DEM contains substantial changes in certain regions, whereas in others there are consistencies between the two DEMs, for example across the Bungenstock ice rise, where there are little new data. The mean error between the two DEMS is -86.45 m indicating a slightly lower bed elevation in the new DEM data compared to Bedmap2, which is likely the result of deep parts of the topography (i.e. valley bottoms) not being visible in the fieldwork non-SAR processed QC radargrams for the IMAFI project

(e.g. Horsehoe Valley, near Patriot Hills in the Ellsworth Mountains (Winter, 2016). The bed elevation measurement upstream of the Bungenstock ice rise and across the Robin Subglacial Basin shows a generally good agreement with Bedmap2; only some portions of new DEM across the Möller Ice Stream and Pirrit Hills area are significantly different from Bedmap2, with differences in bed elevation typically ranging between -109 m to 172 m (Fig. 3c). There is, however, large disagreement between the two DEMs in the western region of Institute Ice Stream, across the Ellsworth Mountains (e.g. in the Horseshoe valley), the Foundation Ice Stream and towards East Antarctica where topography is more rugged. It is also worth noting the significant depth of the bed topography beneath the trunk of the Foundation Ice Stream, where a trough more than ~2 km deep is located and delineated (Fig. 3d). The trough is ~38 km wide and ~80 km in length, with the deepest section ~2.3 km below sea level. The new DEM shows a significant change in the depiction of Foundation Trough; we have measured it to be ~1 km deeper relative to the Bedmap2 product.

In order to further quantify the differences between Bedmap2 and our new DEM, we present terrain profiles of both DEMs relative to four RES flightlines (Fig. 3c). It is worth noting that the new DEM is much more consistent with the bed elevations from the RES data picks compared to Bedmap2 (Fig. 4a and 4b). The new DEM show a correlation coefficient of 0.96 and 0.92 for Profile A and B, respectively. This is slightly higher compared with Bedmap2 which is 0.94 (Profile A) and 0.91 (Profile B), with relative errors of 2% and 1% for Profile A and B, respectively. Although inaccuracies of the bed elevation persist across the Foundation Ice Stream for both DEMs, the gross pattern of the bed elevation for the new DEM is much more consistent with the RES transects relative to Bedmap2 (Fig. 4c and 4d), with correlation coefficients of 0.97 and 0.94 for Profile C and D, respectively. These value contrast with correlation coefficients from Bedmap2 of 0.87 for Profile C and 0.83 for Profile D, with relative errors of 12 and 13%, respectively.

The new DEM can be refined further to deal with bumps and irregularities associated with interpolation effects from along-track data in otherwise data sparse regions. We used the MC technique to infer the bed elevation (Fig. 3e) beneath the fast-moving ice, similar to that successfully employed in Greenland (Morlighem et al., 2017). In general, the bed elevation derived from MC and kriging is consistent with our new DEM. However, using MC significant changes in the bed morphology beneath fast flowing ice occur. For example, using MC, the tributary of the Foundation Ice Stream has been extended for ~100 km further inland relative to our new DEM.

5.2 Hydrology

Computing the potential passageway of subglacial water beneath the ice-sheet is critical for comprehending ice-sheet dynamics (Bell, 2008; Stearns et al., 2008; Siegert et al., 2016a). The development of subglacial hydrology pathways is highly sensitive to ice-surface elevation and, to a lesser degree, by bed morphology (Wright et al., 2008; Horgan et al., 2013). Figure 3d shows a comparison of subglacial hydrology pathways between our new bed DEM and the Bedmap2 DEM. The gross patterns of water flow are largely unchanged between the two DEMs, especially across and upstream of Institute and Möller Ice Streams. The similar water pathway pattern between both DEMs in these regions is also consistent with the small errors in bed topography (Fig. 3c). Despite large differences in bed topography across the Foundation Ice Stream and the Ellsworth Mountains region, the large-scale patterns of water flow are also similar between both DEMs, due to the dominance of the ice-surface slope in driving basal water flow in these regions (Shreve, 1972). Nonetheless, there are several local small-scale differences in the water pathways (Fig. 3d), which highlight hydraulic sensitivity. The subglacial water network observed in the new DEM across the Foundation Ice Stream appears to be more arborescent than that derived from Bedmap2. This is due to the introduction of new data, resulting in a better-defined bed across the Foundation Trough (Fig. 3d). It is also worth noting that the pattern of the subglacial water pathway observed in the new DEM adjacent to the grounding line across the Möller Ice Stream is in good agreement with the position of sub-ice-shelf channels, which have been delineated from a combination of satellite images and RES data (Le Brocq et al., 2013).

Subglacial lakes discovered across the WS sector form an obvious component of the basal hydrological system (Wright and Siegert, 2012). These lakes exist due to sufficient amount of geothermal heating (50 mW m^{-2} – 70 mW m^{-2}), which allows the base of the ice sheet to melt if it is >~2km. In addition, the pressure exerted on the bed by the overlying ice causes the melting point to be lowered. West of the Ellsworth Mountain lies a body of the subglacial water known as Ellsworth Subglacial Lake. The lake measures 28.9 km^2 with a depth ranging between 52 m to 156 m capable of carrying a water body volume of 1.37 km^3 (Woodward et al., 2010). In some cases, ice-surface elevation changes have been linked with subglacial lake hydrological change (Siegert et al., 2016a) – the so called 'active' subglacial lakes. There are 4 known active subglacial lakes distributed across the Institute Ice Stream (Wright and Siegert, 2012): Institute W1 is located close to the Robin Subglacial Basin A whereas Institute W2 is located to the northeast of Pirrit Hill; Institute E1 and E2 are located to the southwest of Robin Subglacial Basin B and near the field camp of C110, respectively. In addition, there are three active subglacial lakes in the Foundation Ice Stream catchment: Foundation 1, Foundation 2, and Foundation 3 (Wright and Siegert, 2012). East of the Foundation Ice Stream, there are 16 active subglacial lakes distributed along the main trunk of Academy Ice Stream (Wright and Siegert, 2012).

5.3 Geomorphological description of the bed topography

The WS sector of WAIS is composed of three major ice-sheet outlets (Fig. 1a); the Institute, Möller and Foundation Ice Streams, feeding ice to the FRIS, the second largest ice shelf in Antarctica after the Ross Ice Shelf. Recent geophysical inspection of the subglacial topography in the region reveals features such as steep reverse bed slopes, similar in scale to that measured for upstream Thwaites Glacier, close to the Institute and Möller Ice Stream grounding lines. The bed slopes inland to a ~1.8 km deep basin (the Robin Subglacial Basin), which is divided into two sections with few obvious significant ice-sheet pinning points (Ross et al., 2012). Elevated beds in other parts of the WS sector allow the ice shelf to ground, causing ice surface features known as ice rises and rumples (Matsuoka et al., 2015).

The Institute Ice Stream has three tributaries, within our survey grid, to the south and west of the Ellsworth Mountains, occupying the Horseshoe Valley, Independence and Ellsworth troughs (Fig. 1b) (Winter et al., 2015). The Horseshoe Valley Trough, around 20 km wide and 1.3 km below sea level at its deepest point, is located downstream of the steep mountains of the Heritage Range. A subglacial ridge is located between the mouth of the Horseshoe Valley Trough and the main trunk of the Institute Ice Stream (Winter et al., 2015). The Independence Trough is located subparallel to the Horseshoe Valley Trough, separated by the 1.4 km high Independence Hills. The trough is ~22 km wide and is 1.1 km below sea level at its deepest point. It is characterized by two distinctive plateaus (~6 km wide each) on each side of the trough, aligned alongside the main trough axis. Ice flows eastward through the Independence Trough for ~54 km before it shifts to a northward direction where the trough widens to 50 km and connects with the main Institute Ice Stream. The Ellsworth Trough is aligned with the Independence Trough, and both are orthogonal to the orientation of the Amundsen – Weddell ice divide, dissecting the Ellsworth Subglacial Highlands northwest to southeast. The Ellsworth Trough measures ~34 km in width and is ~2 km below sea level at its deepest point, and is ~260 km in length. It is considered to be the largest and deepest trough-controlled tributary in this region (Winter et al., 2015). The Ellsworth Trough is intersected by several smaller valleys aligned perpendicularly to the main axis, which are relics landforms from a previous small dynamic ice mass (predating the WAIS in its present configuration) (Ross et al., 2014). The Ellsworth Trough contains ~15 – 20 km long Ellsworth Subglacial Lake (Siegert et al., 2004a; Woodward et al., 2010; Siegert et al., 2012; Wright and Siegert, 2012). It is worth noting that the lake is outside the grid of our DEM.

Satellite altimetry and imagery are able to estimate the grounding line that separates the grounded ice sheet from the floating ice shelf, based on surface changes due to tidal oscillations and the subtle ice surface features. Such analysis is prone to uncertainty, however. There are currently four proposed grounding line locations, based on different satellite data sets and/or methods of analysis (Bohlander and Scambos, 2007; Bindschadler et al., 2011; Brunt et al., 2011; Rignot et al., 2011c). Each of the grounding lines were delineated from satellite images, but without direct measurement of the subglacial environment. This results in ambiguities in the precise location of the transition between floating and grounded ice (Jeofry et al., 2017). In addition, RES data have demonstrated clear errors in the position of the grounding line with a large, hitherto unknown, subglacial embayment near the Institute Ice Stream grounding line. The subglacial embayment is ~1 km deep and is potentially open to the ice shelf cavity, causing the inland ice sheet to have a direct contact with ocean water. In addition, our RES analysis reveals a better- defined Foundation Trough, in which the grounding line is perched on very deep topography around 2 km below sea level.

A previous study revealed a series of ancient large sub-parallel subglacial bed channels between MIS and FIS, adjacent to the Marginal Basins (Fig. 1b) (Rose et al., 2014). While these subglacial channels are likely to have been formed by the flow of basal water, they are presently located beneath slow moving and cold-based ice. It is thought, therefore, that the channels are ancient and were formed at a time when surface melting was prevalent in West Antarctica (e.g. the Pliocene).

The bed topography of the WS appears both rough (over the mountains and exposed bedrock) and smooth (across the sediment-filled regions) (Bingham and Siegert, 2007). Studies of bed roughness calculated using Fast Fourier Transform (FFT) technique based on the relative measurement of bed obstacle amplitude and frequency of the roughness obstacles have indicated that the IIS and MIS are dominated by relatively low roughness values, less than 0.1 (Bingham and Siegert, 2007; Rippin et al., 2014), which was suggested as being the result of the emplacement of marine sediments as in the Siple Coast region (Siegert et al., 2004b; Peters et al., 2005). Radar-derived roughness analysis has evidenced a smooth bed across the Robin Subglacial Basin where sediments may exist (Rippin et al., 2014). The deepest parts of the Robin Subglacial Basin are anomalously rough, marking the edge of a sedimentary drape where the highest ice flow velocities are generated (Siegert et al., 2016b). As such, the smooth basal topography of the Institute and Möller Ice Stream catchments is less extensive than proposed by Bingham and Siegert (2007). It has been demonstrated since, that the subglacial topography of the region between the Robin Subglacial Basin and the Pirrit and Martin-Nash Hills is relatively flat, smooth and gently sloping, and has been interpreted as a bedrock planation surface (Rose et al., 2015). This zone of the study area was originally interpreted by Bingham and Siegert (2009) as underlain by fine-grained marine sediments, due to the limited RES data available to them at the time. Although the exact formation process of the planation surface is unknown, it is thought that this geomorphological feature formed due to marine and/or fluvial erosion (Rose et al., 2015).

6. Data availability

The new 1 km bed elevation product of the Weddell Sea sector, West Antarctica can be found at http://doi.org/10.5281/zenodo.1035488. We used four radar datasets to construct the 1 km ice thickness DEM, as follows: (1) Digitized radar data from the 1970s SPRI-NSF-TUD surveys, in which the bed was picked every 15-20 seconds (1-2 km), recorded here in an Excel 97-2003 Worksheet (XLS), which can be obtained from the UK Polar Data Centre (UKPDC) website at https://data.bas.ac.uk/metadata.php?id=GB/NERC/BAS/AEDC/00326; (2) BAS GRADES/IMAGE and (3) BAS IMAFI airborne surveys, both available from the UKPDC Polar Airborne Geophysics Data Portal at https://secure.antarctica.ac.uk/data/aerogeo/; and (4) NASA Operation IceBridge radar depth sounder Level 2 (L2) data, available from the Center for Remote Sensing of Ice Sheet (CReSIS) website at https://data.cresis.ku.edu/.

The 1 km ice-sheet surface elevation DEM was derived from a combination of ERS-1 surface radar and ICESat laser altimetry, which is downloadable from the National Snow and Ice Data Center (NSIDC) website at https://nsidc.org/data/docs/daac/nsidc0422_antarctic_1km_dem/.

Two-dimensional SAR-processed radargrams in SEG-Y format for the BAS IMAFI airborne survey, and The NASA Operation IceBridge SAR images (Level 1B) in MAT (binary MATLAB) format, are provided at doi.org/10.5285/8a975b9e-f18c-4c519bdb-b00b82da52b8 and https://data.cresis.ku.edu/, respectively.

Ancillary information for the MEaSUREs InSAR-based ice velocity map of Central Antarctica can be found at doi:10.5067/MEASURES/CRYOSPHERE/nsidc-0484.001 and the MODIS Mosaic of Antarctica 2008 – 2009 (MOA2009) ice sheet surface image map is available at doi.org/10.7265/N5KP8037. The RADARSAT (25m) ice-sheet surface satellite imagery is accessible from the Byrd Polar and Climate Research Center website at http://research.bpcrc.osu.edu/rsl/radarsat/data/.

A summary of the data used in this paper, and their availability is provided in the table 1.

7. Conclusions

We have compiled airborne radar data from a number of geophysical surveys, including the SPRI-NSF-TUD surveys of the 1970s, the GRADES/IMAGE and IMAFI surveys acquired by BAS in 2006/7 and 2010/11, respectively, and new geophysical datasets collected by the CReSIS from the NASA OIB project in 2012, 2014 and 2016. From these data, we produce a bed topography DEM with high spatial resolution (1km). The DEM covers a total area of ~125,000 km^2 of the Weddell Sea sector including the Institute, Möller and Foundation ice streams, and the Bungenstock ice rise. Large differences can be observed between the new and previous DEMs (i.e., Bedmap2), most notably across the Foundation Ice Stream where we reveal the grounding line to be resting on a bed ~2 km below sea level, with a deep trough immediately upstream as deep as 2.3 km below sea level. In addition, improved processing of existing data has led to some particularly deep regions of bed to be better resolved than in Bedmap2. Our new DEM also revises the pattern of potential basal water flow across the Foundation Ice Stream and towards East Antarctica in comparison to Bedmap2. Our new DEM, and the data used to compile it, is available to download and will be of value to ice-sheet modelling experiments in which the accuracy of the DEM is important to ice flow processes in this particularly sensitive region of the WAIS.

Author contributions. Hafeez Jeofry carried out the analysis, created the figures and compiled the database. Hafeez Jeofry, Neil Ross and Martin Siegert wrote the paper. All authors contributed to the database compilation, analysis and writing of the paper.

Competing interests. The authors declare that they have no conflict of interest.

Acknowledgement. The data used in this project are available at the Center for the Remote Sensing of Ice data portal https://data.cresis.ku.edu/ and at the UK Airborne Geophysics Data Portal https://secure.antarc-tica.ac.uk/data/aerogeo/. Prasad Gogineni and Jilu Li acknowledge funding by NASA for CReSIS data collection and development of radars (NNX10AT68G), Martin J. Siegert, and Neil Ross acknowledge funding from the NERC Antarctic Funding Initiative (NE/G013071/1) and the IMAFI data collection team consist of Hugh F.J. Corr, Fausto Ferraccioli, Rob Bingham, Anne Le Brocq, David Rippin, Tom Jordan, Carl Robinson, Doug Cochrane, Ian Potten and Mark Oostlander. Hafeez Jeofry acknowledges funding from the Ministry of Higher Education Malaysia, and the Norwegian Polar Institute for the Quantarctica GIS package.

a.

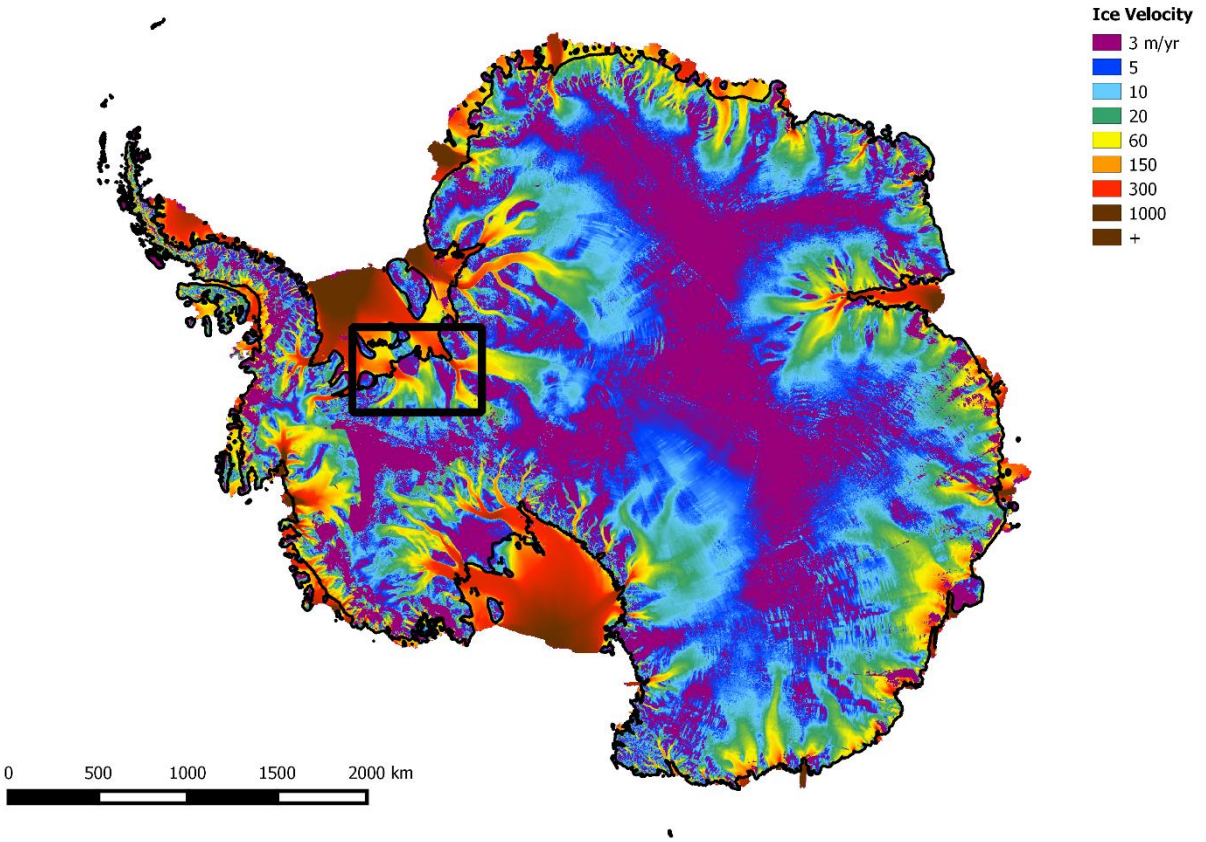
Ice Velocity
3 m/yr
5
10
20
60
150
300
1000
+
0
500
1000
1500
2000 km

b.

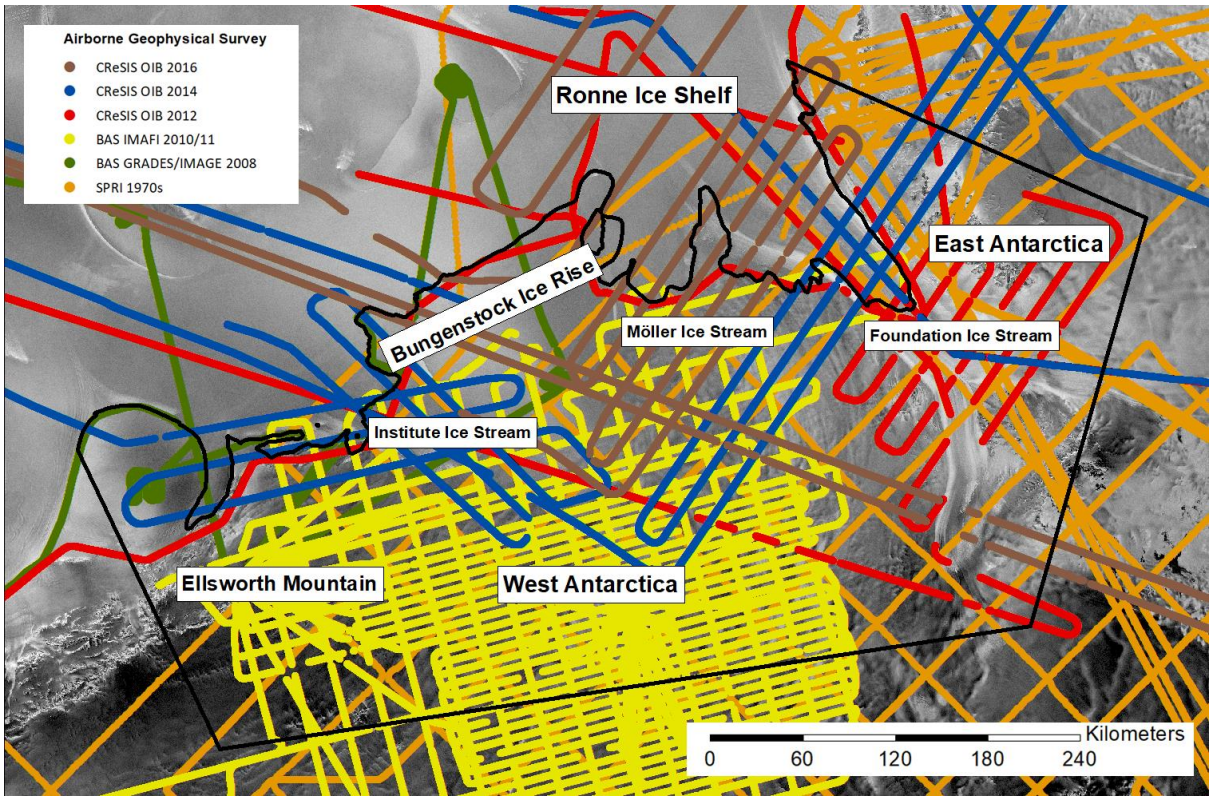
Airborne Geophysical Survey
CReSIS OIB 2016
CReSIS OIB 2014
CReSIS OIB 2012
BAS IMAFI 2010/11
BAS GRADES/IMAGE 2008
SPRI 1970s
Ronne Ice Shelf
East Antarctica
Bungenstock Ice Rise
Möller Ice Stream
Foundation Ice Stream
Institute Ice Stream
Ellsworth Mountain
West Antarctica
Kilometers
0
60
120
180
240

c.

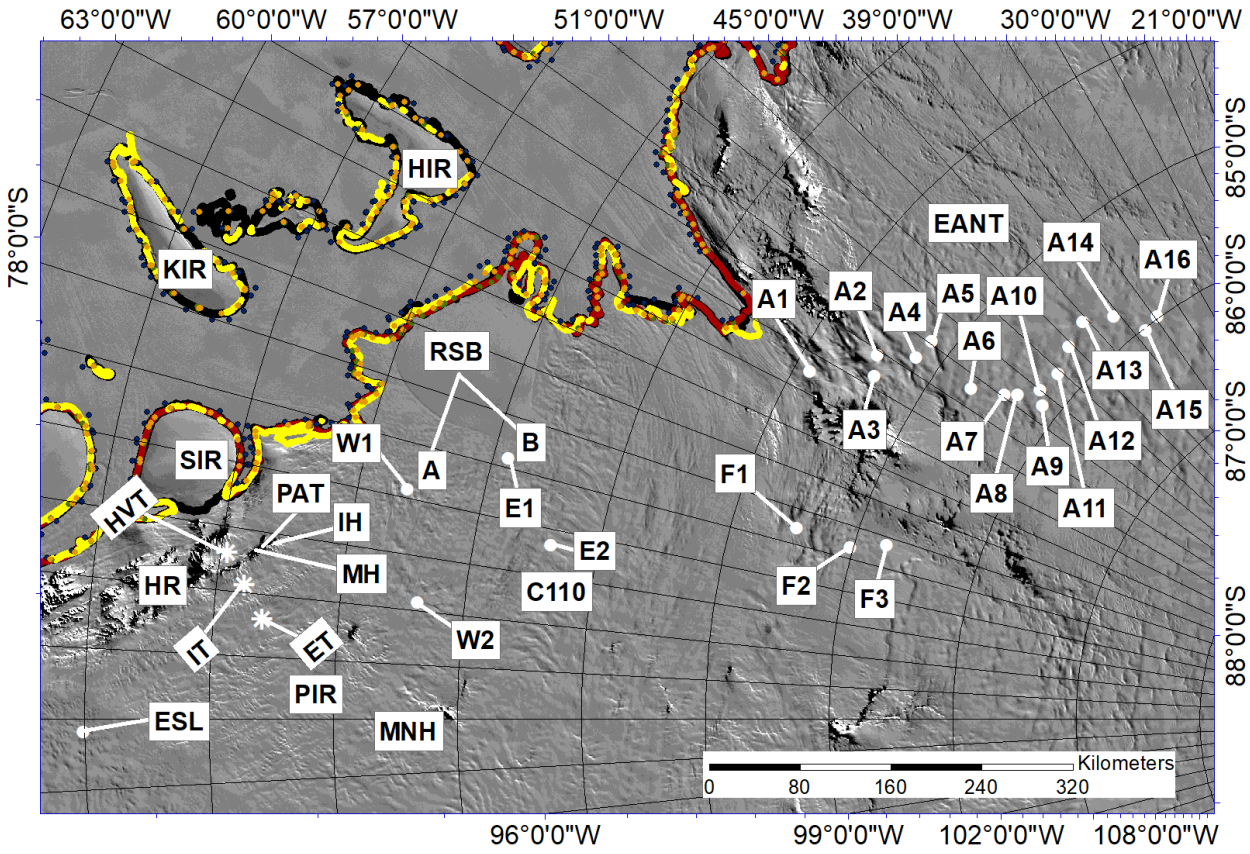

Figure 1. Map of: (a) A location inset of Antarctica overlain with InSAR-derived ice surface velocities (Rignot et al., 2011d); (b)The aerogeophysical flight lines across Weddell Sea sector superimposed over RADARSAT (25m) satellite imagery mosaic (Jezek, 2002); SPRI airborne survey 1969 – 1979 (orange); BAS GRADES/IMAGE survey 2008 (green); BAS Institute Ice Stream survey 2010/2011 (IMAFI) (yellow); OIB 2012 (red); OIB 2014 (blue); and OIB 2016 (brown); (c) Map of the Weddell Sea sector on MODIS imagery (Haran et al., 2014) with grounding lines superimposed on the map; ICESat laser altimetry (blue: hydrostatic point; orange: ice flexure landward limit; green: break-in-slope) grounding line (Brunt et al., 2010); Antarctic Surface Accumulation and Ice Discharge (ASAID) grounding line (red line) (Bindschadler et al., 2011); Mosaic of Antarctic (MOA) grounding line (black line) (Bohlander and Scambos, 2007); and Differential Synthetic Aperture Radar Interferometry (DInSAR) grounding line (Rignot et al., 2011a); Annotations: KIR – Korff ice rise; HIR – Henry ice rise; SIR – Skytrain ice rise; HR – Heritage Range; HVT – Horseshoe Valley Trough; IT – Independence Trough; ET – Ellsworth Trough; ESL – Ellsworth Subglacial Lake; E1 – Institute E1 Subglacial Lake; E2 – Institute E2 Subglacial Lake; A1 – Academy 1 Subglacial Lake; A2 – Academy 2 Subglacial Lake; A3 – Academy 3 Subglacial Lake; A4 – Academy 4 Subglacial Lake; A5 – Academy 5 Subglacial Lake; A6 – Academy 6 Subglacial Lake; A7 – Academy 7 Subglacial Lake; A8 – Academy 8 Subglacial Lake; A9 – Academy 9 Subglacial Lake; A10 – Academy 10 Subglacial Lake; A11 – Academy 11 Subglacial Lake; A12 – Academy 12 Subglacial Lake; A13 – Academy 13 Subglacial Lake; A14 – Academy 14 Subglacial Lake; A15 – Academy 15 Subglacial Lake; A16 – Academy 16 Subglacial Lake; A17 – Academy 17 Subglacial Lake; W1 – Institute W1 Subglacial Lake; W2 Institute W2 Subglacial Lake; F1 – Foundation 1 Subglacial Lake; F2 – Foundation 2 Subglacial Lake; F3 – Foundation 3 Subglacial Lake; PAT – Patriot Hills; IH – Independence Hills; MH – Marble Hills; PIR – Pirrit Hills; MNH – Martin-Nash Hills; RSB – Robin Subglacial Basin; and EANT – East Antarctica.

a.

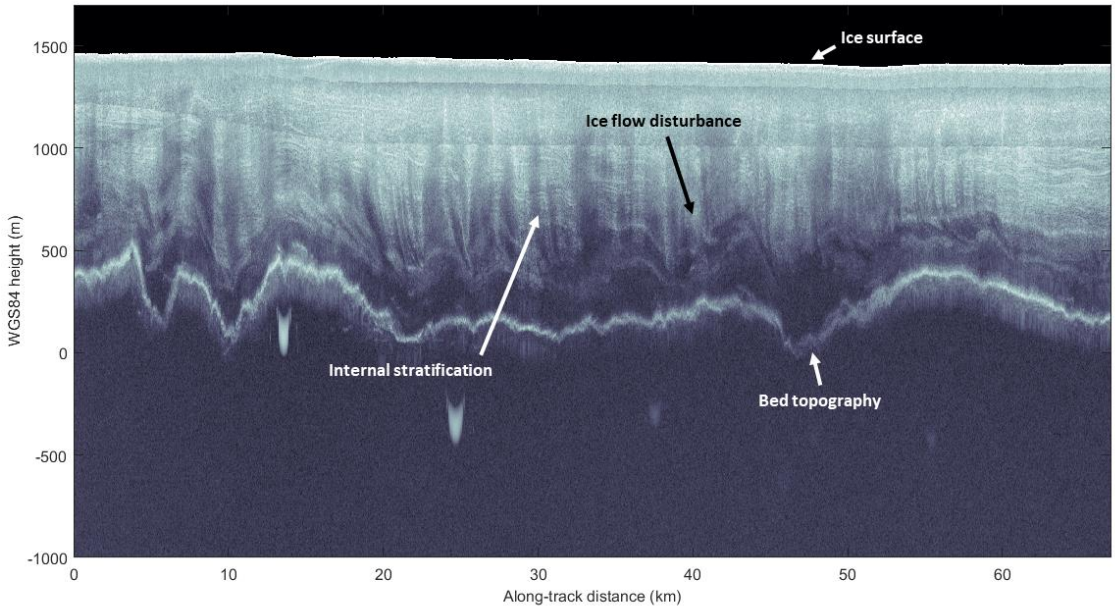

b.

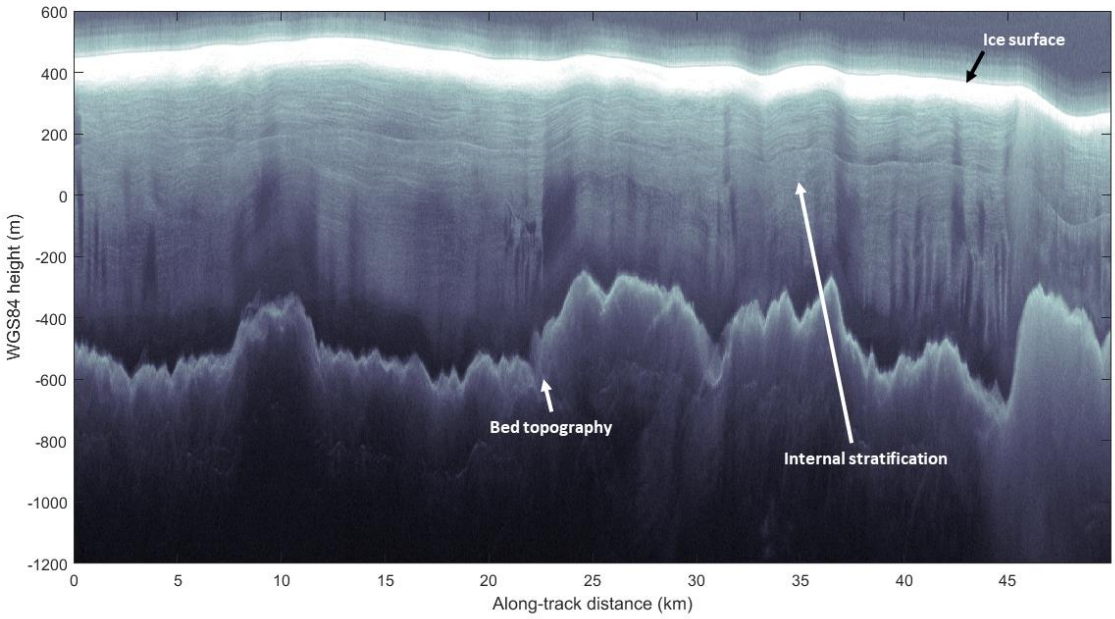

Figure 2. Two-dimensional synthetic aperture radar (SAR) processed radargrams of: (a) BAS IMAFI data (b) OIB data.

a.

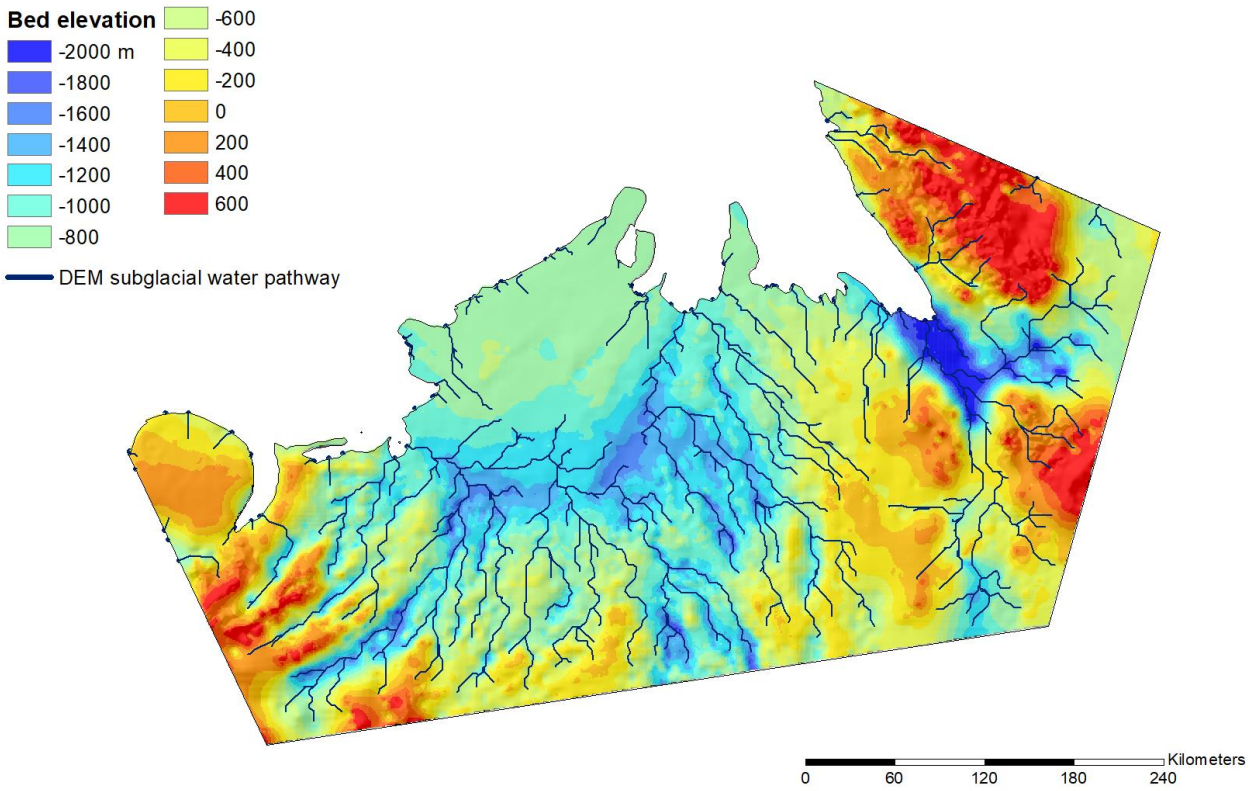
Bed elevation
-2000 m
-1800
-1600
-1400
-1200
-1000
-800
-600
-400
-200
0
200
400
600
DEM subglacial water pathway
Kilometers
0
60
120
180
240

b.

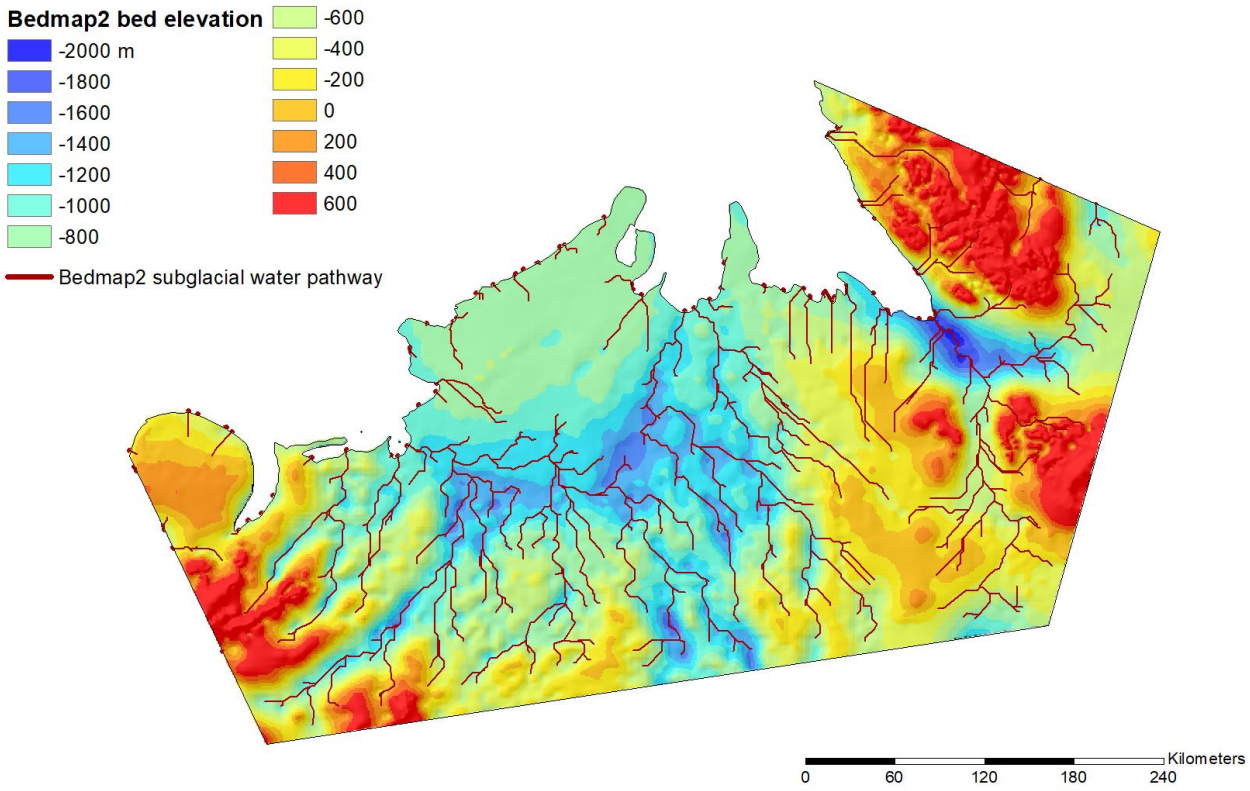
Bedmap2 bed elevation
-2000 m
-1800
-1600
-1400
-1200
-1000
-800
-600
-400
-200
0
200
400
600
Bedmap2 subglacial water pathway
Kilometers
0
60
120
180
240

c.

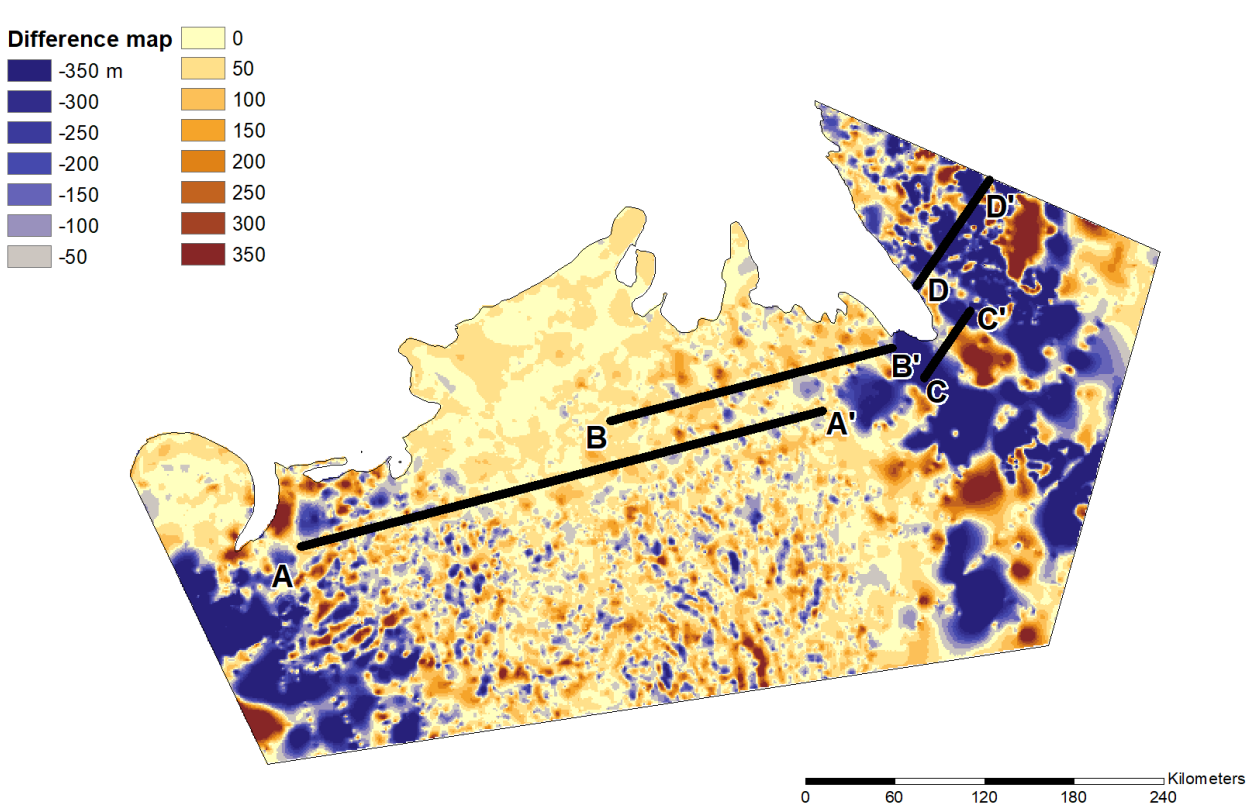
Difference map
-350 m
-300
-250
-200
-150
-100
-50
0
50
100
150
200
250
300
350
A
A'
B
B'
C
C'
D
D'
0
60
120
180
240
Kilometers

d.

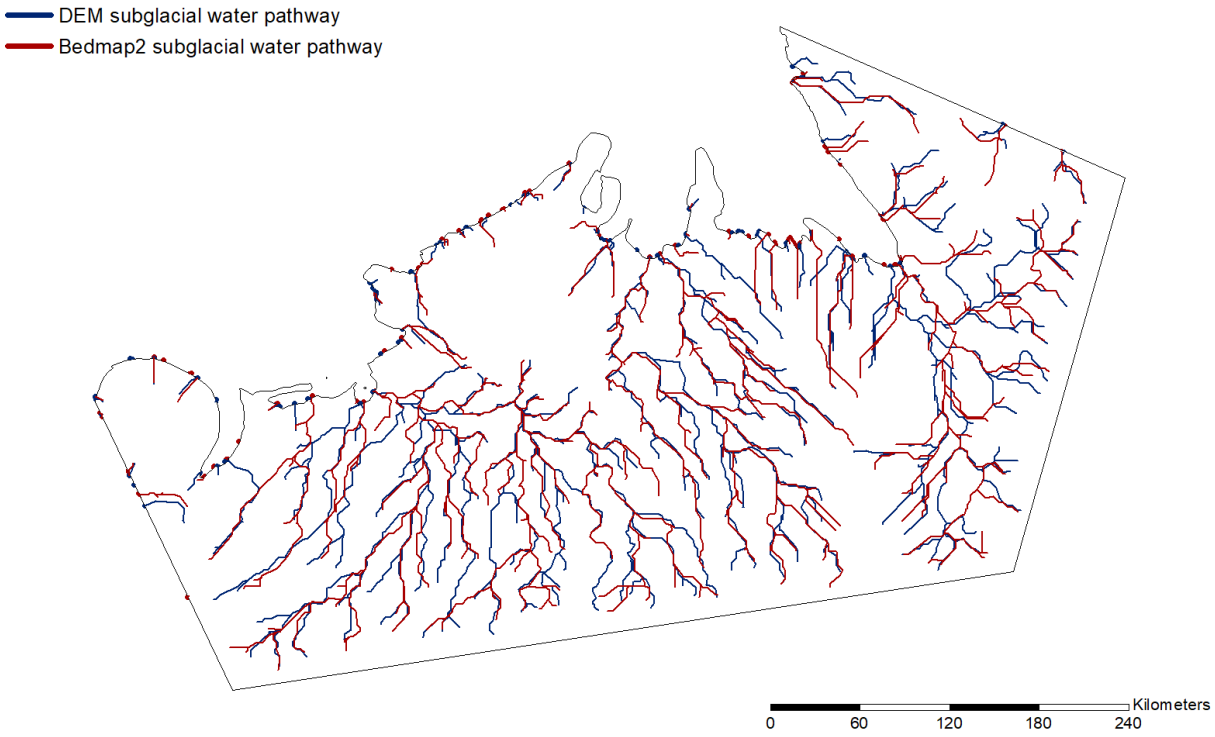
DEM subglacial water pathway
Bedmap2 subglacial water pathway
0
60
120
180
240
Kilometers

e.

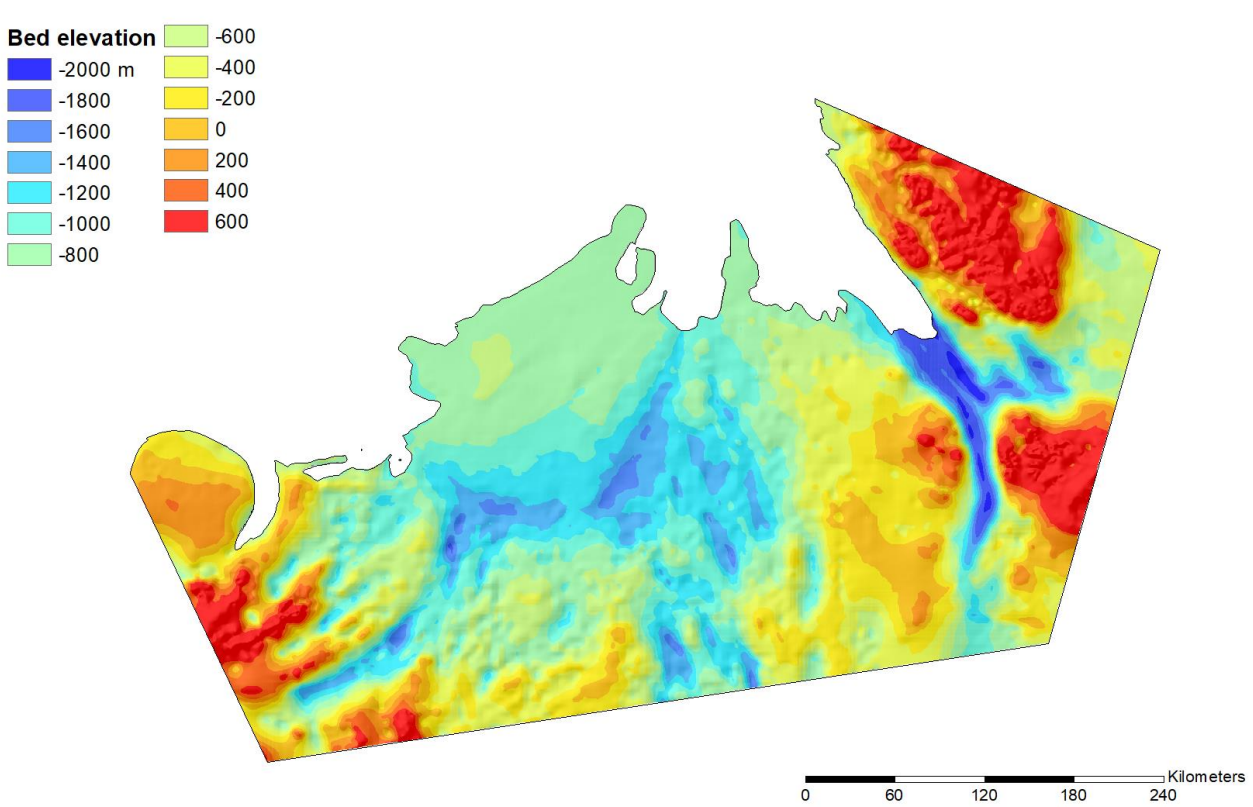

Figure 3. Map of: (a) A new bed topography digital elevation model; (b) Bedmap2 bed elevation product (Fretwell et al., 2013); (c) Profile A – A', B – B', C – C' and D – D' overlain by map showing differences in bed elevation between the new DEM and Bedmap2; (d) DEM and Bedmap2 subglacial water pathway; and (e) bed topography digital elevation model inferred using mass conservation and kriging.

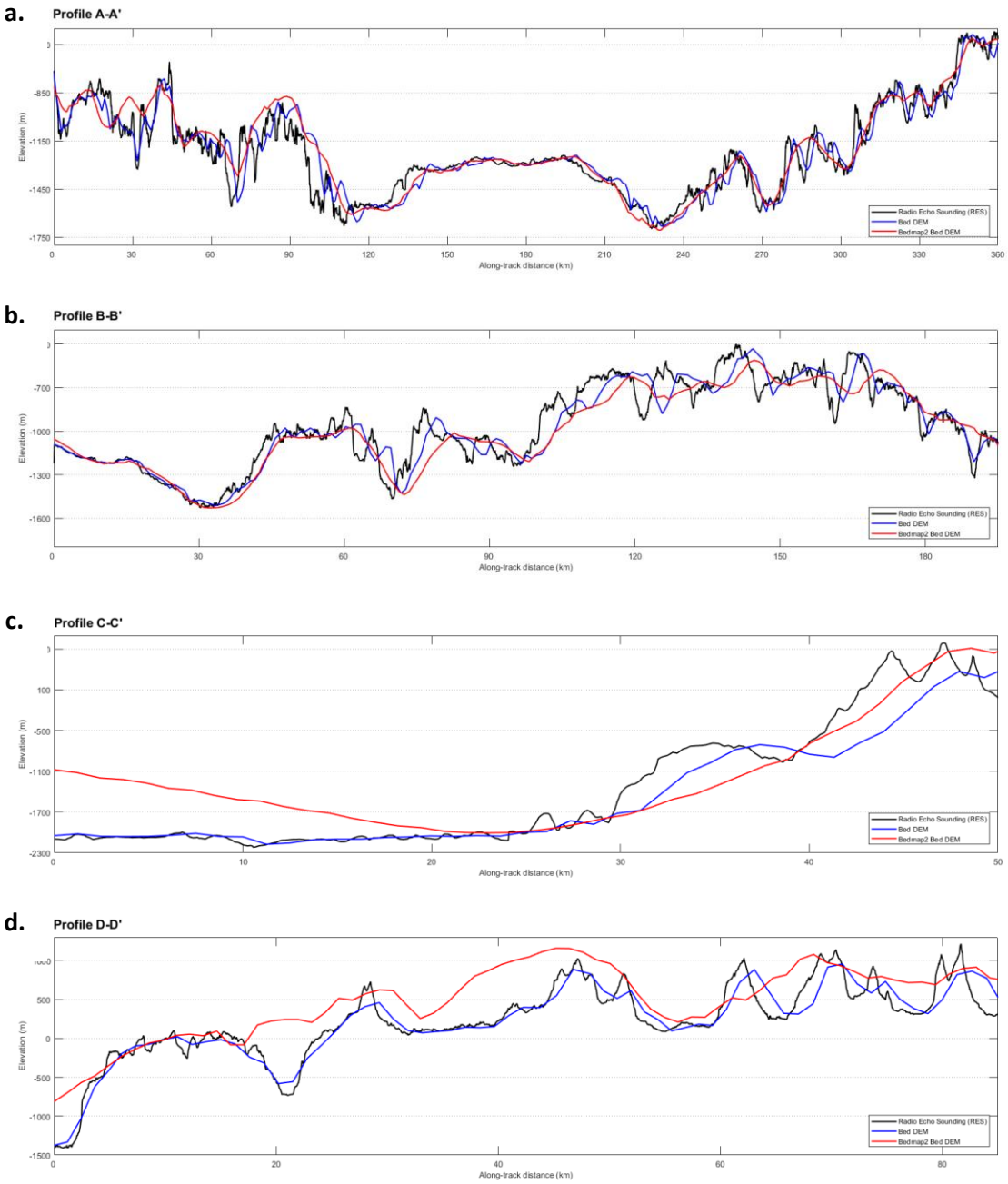

Figure 4. Bed elevation for the RES transect (black), DEM (blue) and Bedmap2 (red) of: (a) Profile A – A'; (b) Profile B – B'; (c) Profile C – C'; and (d) Profile D – D'.

Table 1: Data files and locations.

Products	Files	Location	DOI/URL
1-km bed elevation DEM	1-km bed elevation DEM	Zenodo Data Repository	http://doi.org/10.5281/zenodo.1035488
1-km ice thickness DEM	Digitized SPRI-NSF-TUD bed picks data	UK Polar Data Centre (UKPDC)	https://data.bas.ac.uk/metadata.php?id=GB/NERC/BAS/AEDC/00326
	BAS GRADES/IMAGE ice thickness data	UK Polar Data Centre (UKPDC)	https://secure.antarctica.ac.uk/data/aerogeo/
	BAS IMAFI ice thickness data	UK Polar Data Centre (UKPDC)	https://secure.antarctica.ac.uk/data/aerogeo/
	NASA Operation IceBridge radar depth sounder Level 2 (L2) data	Center for Remote Sensing of Ice Sheet (CReSIS)	https://data.cresis.ku.edu/
1-km ice sheet surface DEM	ERS-1 radar and ICESat laser satellite altimetry	National Snow and Ice Data Center (NSIDC)	https://nsidc.org/data/docs/daac/nsidc0422_antarctic_1km_dem/
Two-dimensional synthetic aperture radar (SAR) processed radargrams	BAS IMAFI airborne survey	UK Polar Data Centre (UKPDC)	doi.org/10.5285/8a975b9e-f18c-4c51-9bdb-b00b82da52b8
	NASA Operation IceBridge airborne survey	Center for Remote Sensing of Ice Sheet (CReSIS)	https://data.cresis.ku.edu/
Ice velocity map of Central Antarctica	MEaSUREs InSAR-based ice velocity	National Snow and Ice Data Center (NSIDC)	doi:10.5067/MEASURES/CRYOSPHERE/nsidc-0484.001
Ice sheet surface satellite imagery	MODIS Mosaic of Antarctica (2008 – 2009) (MOA2009)	National Snow and Ice Data Center (NSIDC)	doi.org/10.7265/N5KP8037
	RADARSAT (25m) satellite imagery	Byrd Polar and Climate Research Center	http://research.bpcrc.osu.edu/rsl/radarsat/data/

References

Ashmore, D. W., Bingham, R. G., Hindmarsh, R. C., Corr, H. F., and Joughin, I. R.: The relationship between sticky spots and radar reflectivity beneath an active West Antarctic ice stream, Annals of Glaciology, 55, 29-38, 2014.

Bamber, J., Gomez-Dans, J., and Griggs, J.: Antarctic 1 km digital elevation model (DEM) from combined ERS-1 radar and ICESat laser satellite altimetry, National Snow and Ice Data Center, Boulder, 2009a. 2009a.

Bamber, J. L., Riva, R. E., Vermeersen, B. L., and LeBrocq, A. M.: Reassessment of the potential sea-level rise from a collapse of the West Antarctic Ice Sheet, Science, 324, 901-903, 2009b.

Bell, R. E.: The role of subglacial water in ice-sheet mass balance, Nature Geoscience, 1, 297-304, 2008.

Bindschadler, R., Choi, H., and Collaborators, A.: High-resolution image-derived grounding and hydrostatic lines for the Antarctic Ice Sheet, Digital media, National Snow and Ice Data Center, Boulder, Colorado, USA, 2011. 2011.

Bingham, R. G. and Siegert, M. J.: Quantifying subglacial bed roughness in Antarctica: implications for ice-sheet dynamics and history, Quaternary Science Reviews, 28, 223-236, 2009.

Bingham, R. G. and Siegert, M. J.: Radar-derived bed roughness characterization of Institute and Möller ice streams, West Antarctica, and comparison with Siple Coast ice streams, Geophysical Research Letters, 34, 2007.

Bohlander, J. and Scambos, T.: Antarctic coastlines and grounding line derived from MODIS Mosaic of Antarctica (MOA), National Snow and Ice Data Center, Boulder, CO, USA, 2007. 2007.

Brunt, K. M., Fricker, H. A., and Padman, L.: Analysis of ice plains of the Filchner–Ronne Ice Shelf, Antarctica, using ICESat laser altimetry, Journal of Glaciology, 57, 965-975, 2011.

Brunt, K. M., Fricker, H. A., Padman, L., Scambos, T. A., and O'Neel, S.: Mapping the grounding zone of the Ross Ice Shelf, Antarctica, using ICESat laser altimetry, Annals of Glaciology, 51, 71-79, 2010.

Budd, W., Jenssen, D., and Smith, I.: A three-dimensional time-dependent model of the West Antarctic ice sheet, Annals of Glaciology, 5, 29-36, 1984.

Christensen, E. L.: Radioglaciology 300 MHz radar, Technical University [of] Denmark, Electromagnetics Institute, 1970.

Corr, H. F., Ferraccioli, F., Frearson, N., Jordan, T., Robinson, C., Armadillo, E., Caneva, G., Bozzo, E., and Tabacco, I.: Airborne radio-echo sounding of the Wilkes Subglacial Basin, the Transantarctic Mountains and the Dome C region, Terra Antartica Reports, 13, 55-63, 2007.

Dowdeswell, J. A. and Evans, S.: Investigations of the form and flow of ice sheets and glaciers using radio-echo sounding, Reports on Progress in Physics, 67, 1821, 2004.

Drewry, D. and Meldrum, D.: Antarctic airborne radio echo sounding, 1977–78, Polar Record, 19, 267-273, 1978.

Drewry, D., Meldrum, D., and Jankowski, E.: Radio echo and magnetic sounding of the Antarctic ice sheet, 1978–79, Polar Record, 20, 43-51, 1980.

Drewry, D. J.: Antarctica, Glaciological and Geophysical Folio, University of Cambridge, Scott Polar Research Institute, 1983.

Fretwell, P., Pritchard, H. D., Vaughan, D. G., Bamber, J. L., Barrand, N. E., Bell, R., Bianchi, C., Bingham, R. G., Blankenship, D. D., Casassa, G., Catania, G., Callens, D., Conway, H., Cook, A. J., Corr, H. F. J., Damaske, D., Damm, V., Ferraccioli, F., Forsberg, R., Fujita, S., Gim, Y., Gogineni, P., Griggs, J. A., Hindmarsh, R. C. A., Holmlund, P., Holt, J. W., Jacobel, R. W., Jenkins, A., Jokat, W., Jordan, T., King, E. C., Kohler, J., Krabill, W., Riger-Kusk, M., Langley, K. A., Leitchenkov, G., Leuschen, C., Luyendyk, B. P., Matsuoka, K., Mouginot, J., Nitsche, F. O., Nogi, Y., Nost, O. A., Popov, S. V., Rignot, E., Rippin, D. M., Rivera, A., Roberts, J., Ross, N., Siegert, M. J., Smith, A. M., Steinhage, D., Studinger, M., Sun, B., Tinto, B. K., Welch, B. C., Wilson, D., Young, D. A., Xiangbin, C., and Zirizzotti, A.: Bedmap2: improved ice bed, surface and thickness datasets for Antarctica, The Cryosphere, 7, 375-393, 2013.

Gogineni, P.: CReSIS Radar Depth Sounder Data, Lawrence, Kansas, USA, Digital Media, http://data.cresis.ku.edu/, 2012. 2012.

Gogineni, S., Yan, J.-B., Paden, J., Leuschen, C., Li, J., Rodriguez-Morales, F., Braaten, D., Purdon, K., Wang, Z., and Liu, W.: Bed topography of Jakobshavn Isbræ, Greenland, and Byrd Glacier, Antarctica, Journal of Glaciology, 60, 813-833, 2014.

Graham, F. S., Roberts, J. L., Galton-Fenzi, B. K., Young, D., Blankenship, D., and Siegert, M. J.: A high-resolution synthetic bed elevation grid of the Antarctic continent, Earth System Science Data Discussions, doi: 10.5194/essd-2016-18, 2016. 1-18, 2016.

Haran, T., Bohlander, J., Scambos, T., Painter, T., and Fahnestock, M.: MODIS Mosaic of Antarctica 2008–2009 (MOA2009) Image Map, Boulder, Colorado USA: National Snow and Ice Data Center, do i, 10, N5KP8037, 2014.

Harry, L. and Trees, V.: Optimum array processing: part IV of detection, estimation, and modulation theory, John Wiley and Sons, Inc, 2002. 2002.
Hélière, F., Lin, C.-C., Corr, H., and Vaughan, D.: Radio echo sounding of Pine Island Glacier, West Antarctica: Aperture synthesis processing and analysis of feasibility from space, IEEE Transactions on Geoscience and Remote Sensing, 45, 2573-2582, 2007.
Hellmer, H. H., Kauker, F., Timmermann, R., Determann, J., and Rae, J.: Twenty-first-century warming of a large Antarctic ice-shelf cavity by a redirected coastal current, Nature, 485, 225-228, 2012.
Horgan, H. J., Alley, R. B., Christianson, K., Jacobel, R. W., Anandakrishnan, S., Muto, A., Beem, L. H., and Siegfried, M. R.: Estuaries beneath ice sheets, Geology, 41, 1159-1162, 2013.
Hutchinson, M. F.: Calculation of hydrologically sound digital elevation models, August 17-19 1988, 117-133, 1988.
Jacobs, S. S., Jenkins, A., Giulivi, C. F., and Dutrieux, P.: Stronger ocean circulation and increased melting under Pine Island Glacier ice shelf, Nature Geoscience, 4, 519-523, 2011.
Jankowski, E. J. and Drewry, D.: The structure of West Antarctica from geophysical studies, Nature, 291, 17-21, 1981.
Jeofry, H., Ross, N., Corr, H. F., Li, J., Gogineni, P., and Siegert, M. J.: A deep subglacial embayment adjacent to the grounding line of Institute Ice Stream, West Antarctica, Geological Society, London, Special Publications, 461, SP461. 411, 2017.
Jezek, K. C.: RADARSAT-1 Antarctic Mapping Project: change-detection and surface velocity campaign, Annals of Glaciology, 34, 263-268, 2002.
Jordan, T. A., Ferraccioli, F., Ross, N., Corr, H. F. J., Leat, P. T., Bingham, R. G., Rippin, D. M., le Brocq, A., and Siegert, M. J.: Inland extent of the Weddell Sea Rift imaged by new aerogeophysical data, Tectonophysics, 585, 137-160, 2013.
Le Brocq, A., Payne, A. J., and Vieli, A.: An improved Antarctic dataset for high resolution numerical ice sheet models (ALBMAP v1), Earth System Science Data, 2, 247-260, 2010.
Le Brocq, A., Ross, N., Griggs, J. A., Bingham, R. G., Corr, H. F., Ferraccioli, F., Jenkins, A., Jordan, T. A., Payne, A. J., and Rippin, D. M.: Evidence from ice shelves for channelized meltwater flow beneath the Antarctic Ice Sheet, Nature Geoscience, 6, 945-948, 2013.
Lindbäck, K., Pettersson, R., Doyle, S. H., Helanow, C., Jansson, P., Kristensen, S. S., Stenseng, L., Forsberg, R., and Hubbard, A. L.: High-resolution ice thickness and bed topography of a land-terminating section of the Greenland Ice Sheet, Earth System Science Data, 6, 331-338, 2014.
Lythe, M. B. and Vaughan, D. G.: BEDMAP: A new ice thickness and subglacial topographic model of Antarctica, Journal of Geophysical Research: Solid Earth, 106, 11335-11351, 2001.
Martin, M. A., Levermann, A., and Winkelmann, R.: Comparing ice discharge through West Antarctic Gateways: Weddell vs. Amundsen Sea warming, The Cryosphere Discussions, 9, 1705-1733, 2015.
Matsuoka, K., Hindmarsh, R. C. A., Moholdt, G., Bentley, M. J., Pritchard, H. D., Brown, J., Conway, H., Drews, R., Durand, G., Goldberg, D., Hattermann, T., Kingslake, J., Lenaerts, J. T. M., Martín, C., Mulvaney, R., Nicholls, K. W., Pattyn, F., Ross, N., Scambos, T., and Whitehouse, P. L.: Antarctic ice rises and rumples: Their properties and significance for ice-sheet dynamics and evolution, Earth-Science Reviews, 150, 724-745, 2015.
Morlighem, M., Rignot, E., Seroussi, H. l., Larour, E., Ben Dhia, H., and Aubry, D.: A mass conservation approach for mapping glacier ice thickness, Geophysical Research Letters, 38, 2011.
Morlighem, M., Williams, C., Rignot, E., An, L., Arndt, J. E., Bamber, J. L., Catania, G., ChauchÃ©, N., Dowdeswell, J. A., and Dorschel, B.: BedMachine v3: Complete bed topography and ocean bathymetry mapping of Greenland from multibeam echo sounding combined with mass conservation, Geophysical Research Letters, 2017. 2017.
Peters, M. E., Blankenship, D. D., and Morse, D. L.: Analysis techniques for coherent airborne radar sounding: Application to West Antarctic ice streams, Journal of Geophysical Research: Solid Earth, 110, 2005.
Plewes, L. A. and Hubbard, B.: A review of the use of radio-echo sounding in glaciology, Progress in Physical Geography, 25, 203-236, 2001.
Pritchard, H. D.: Bedgap: where next for Antarctic subglacial mapping?, Antarctic Science, 26, 742, 2014.
Rignot, E., Mouginot, J., and Scheuchl, B.: Antarctic grounding line mapping from differential satellite radar interferometry, Geophysical Research Letters, 38, n/a-n/a, 2011a.
Rignot, E., Mouginot, J., and Scheuchl, B.: Ice flow of the Antarctic ice sheet, Science, 333, 1427-1430, 2011b.
Rignot, E., Mouginot, J., and Scheuchl, B.: MEaSUREs Antarctic Grounding Line from Differential Satellite Radar Interferometry, National Snow and Ice Data Center: Boulder, CO, USA, 2011c. 2011c.

552 Rignot, E., Mouginot, J., and Scheuchl, B.: MEaSUREs InSAR-based Antarctica ice velocity map, National Snow
553 and Ice Data Center: Boulder, CO, USA, 2011d. 2011d.
554 Rippin, D., Bingham, R., Jordan, T., Wright, A., Ross, N., Corr, H., Ferraccioli, F., Le Brocq, A., Rose, K., and
555 Siegert, M.: Basal roughness of the Institute and Möller Ice Streams, West Antarctica: Process determination
556 and landscape interpretation, Geomorphology, 214, 139-147, 2014.
557 Ritz, C., Edwards, T. L., Durand, G., Payne, A. J., Peyaud, V., and Hindmarsh, R. C.: Potential sea-level rise from
558 Antarctic ice-sheet instability constrained by observations, Nature, 528, 115-118, 2015.
559 Rodriguez-Morales, F., Gogineni, S., Leuschen, C. J., Paden, J. D., Li, J., Lewis, C. C., Panzer, B., Alvestegui, D. G.-
560 G., Patel, A., and Byers, K.: Advanced multifrequency radar instrumentation for polar research, IEEE
561 Transactions on Geoscience and Remote Sensing, 52, 2824-2842, 2014.
562 Rose, K. C., Ross, N., Bingham, R. G., Corr, H. F. J., Ferraccioli, F., Jordan, T. A., Le Brocq, A. M., Rippin, D. M., and
563 Siegert, M. J.: A temperate former West Antarctic ice sheet suggested by an extensive zone of subglacial
564 meltwater channels, Geology, 42, 971-974, 2014.
565 Rose, K. C., Ross, N., Jordan, T. A., Bingham, R. G., Corr, H. F., Ferraccioli, F., Le Brocq, A. M., Rippin, D. M., and
566 Siegert, M. J.: Ancient pre-glacial erosion surfaces preserved beneath the West Antarctic Ice Sheet, Earth
567 Surface Dynamics, 3, 139, 2015.
568 Ross, N., Bingham, R. G., Corr, H. F. J., Ferraccioli, F., Jordan, T. A., Le Brocq, A., Rippin, D. M., Young, D.,
569 Blankenship, D. D., and Siegert, M. J.: Steep reverse bed slope at the grounding line of the Weddell Sea sector in
570 West Antarctica, Nature Geoscience, 5, 393-396, 2012.
571 Ross, N., Jordan, T. A., Bingham, R. G., Corr, H. F., Ferraccioli, F., Le Brocq, A., Rippin, D. M., Wright, A. P., and
572 Siegert, M. J.: The Ellsworth subglacial highlands: inception and retreat of the West Antarctic Ice Sheet,
573 Geological Society of America Bulletin, 126, 3-15, 2014.
574 Shi, L., Allen, C. T., Ledford, J. R., Rodriguez-Morales, F., Blake, W. A., Panzer, B. G., Prokopiack, S. C., Leuschen,
575 C. J., and Gogineni, S.: Multichannel coherent radar depth sounder for NASA operation ice bridge, 2010, 1729-
576 1732.
577 Shreve, R.: Movement of water in glaciers, Journal of Glaciology, 11, 205-214, 1972.
578 Siegert, M. J.: On the origin, nature and uses of Antarctic ice-sheet radio-echo layering, Progress in Physical
579 Geography, 23, 159-179, 1999.
580 Siegert, M. J., Clarke, R. J., Mowlem, M., Ross, N., Hill, C. S., Tait, A., Hodgson, D., Parnell, J., Tranter, M., and
581 Pearce, D.: Clean access, measurement, and sampling of Ellsworth Subglacial Lake: a method for exploring deep
582 Antarctic subglacial lake environments, Reviews of Geophysics, 50, 2012.
583 Siegert, M. J., Hindmarsh, R., Corr, H., Smith, A., Woodward, J., King, E. C., Payne, A. J., and Joughin, I.: Subglacial
584 Lake Ellsworth: A candidate for in situ exploration in West Antarctica, Geophysical Research Letters, 31, 2004a.
585 Siegert, M. J., Ross, N., Corr, H., Smith, B., Jordan, T., Bingham, R., Ferraccioli, F., Rippin, D., and Le Brocq, A.:
586 Boundary conditions of an active West Antarctic subglacial lake: implications for storage of water beneath the
587 ice sheet, 2014. 2014.
588 Siegert, M. J., Ross, N., and Le Brocq, A. M.: Recent advances in understanding Antarctic subglacial lakes and
589 hydrology, Phil. Trans. R. Soc. A, 374, 20140306, 2016a.
590 Siegert, M. J., Ross, N., Li, J., Schroeder, D. M., Rippin, D., Ashmore, D., Bingham, R., and Gogineni, P.: Subglacial
591 controls on the flow of Institute Ice Stream, West Antarctica, Annals of Glaciology, 2016b. 1-6, 2016b.
592 Siegert, M. J., Taylor, J., Payne, A. J., and Hubbard, B.: Macro-scale bed roughness of the siple coast ice streams
593 in West Antarctica, Earth Surface Processes and Landforms, 29, 1591-1596, 2004b.
594 Skou, N. and Søndergaard, F.: Radioglaciology. A 60 MHz ice sounder system, Technical University of Denmark,
595 1976.
596 Snyder, J. P.: Map projections--A working manual, US Government Printing Office, Washington, D.C., 1987.
597 Stearns, L. A., Smith, B. E., and Hamilton, G. S.: Increased flow speed on a large East Antarctic outlet glacier
598 caused by subglacial floods, Nature Geoscience, 1, 827-831, 2008.
599 Stocker, T.: Climate change 2013: the physical science basis: Working Group I contribution to the Fifth
600 assessment report of the Intergovernmental Panel on Climate Change, Cambridge University Press, 2014.
601 Thoma, M., Determann, J., Grosfeld, K., Goeller, S., and Hellmer, H. H.: Future sea-level rise due to projected
602 ocean warming beneath the Filchner Ronne Ice Shelf: A coupled model study, Earth and Planetary Science
603 Letters, 431, 217-224, 2015.
604 Van Wessem, J., Reijmer, C., Morlighem, M., Mouginot, J., Rignot, E., Medley, B., Joughin, I., Wouters, B.,
605 Depoorter, M., and Bamber, J.: Improved representation of East Antarctic surface mass balance in a regional
606 atmospheric climate model, Journal of Glaciology, 60, 761-770, 2014.

607 Winter, K.: Englacial stratigraphy, debris entrainment and ice sheet stability of Horseshoe Valley, West
608 Antarctica, 2016.Doctoral thesis, University of Northumbria, Newcastle upon Tyne, England, UK, 263 pp., 2016.
609 Winter, K., Woodward, J., Ross, N., Dunning, S. A., Bingham, R. G., Corr, H. F. J., and Siegert, M. J.: Airborne
610 radar evidence for tributary flow switching in Institute Ice Stream, West Antarctica: Implications for ice sheet
611 configuration and dynamics, Journal of Geophysical Research: Earth Surface, 120, 1611-1625, 2015.
612 Woodward, J., Smith, A. M., Ross, N., Thoma, M., Corr, H., King, E. C., King, M., Grosfeld, K., Tranter, M., and
613 Siegert, M.: Location for direct access to subglacial Lake Ellsworth: An assessment of geophysical data and
614 modeling, Geophysical Research Letters, 37, 2010.
615 Wright, A. and Siegert, M.: A fourth inventory of Antarctic subglacial lakes, Antarctic Science, 24, 659-664, 2012.
616 Wright, A., Siegert, M., Le Brocq, A., and Gore, D.: High sensitivity of subglacial hydrological pathways in
617 Antarctica to small ice-sheet changes, Geophysical Research Letters, 35, 2008.
618 Wright, A. P., Le Brocq, A. M., Cornford, S. L., Bingham, R. G., Corr, H. F. J., Ferraccioli, F., Jordan, T. A., Payne, A.
619 J., Rippin, D. M., Ross, N., and Siegert, M. J.: Sensitivity of the Weddell Sea sector ice streams to sub-shelf
620 melting and surface accumulation, The Cryosphere, 8, 2119-2134, 2014.